Rubidium isotopic fractionation during magmatic processes and the composition of the bulk silicate Earth

Baoliang Wang, Frederic Moynier, Matthew G. Jackson, Fang Huang, Xia Hu, Sæmundur Ari Halldórsson, Wei Dai, Gabriel Devos

Version of Record: https://www.sciencedirect.com/science/article/pii/S0016703723002399
Manuscript_095d354c476fb62c56ce760e272e691c

Rubidium isotopic fractionation during magmatic processes and the composition of the bulk silicate Earth

Baoliang Wang[1, *], Frederic Moynier[1], Matthew G. Jackson[2], Fang Huang[3], Xia Hu[3], Sæmundur Ari Halldórsson[4], Wei Dai[1], Gabriel Devos[1]

[1]Université Paris Cité, Institut de Physique du Globe de Paris, CNRS, 1 Rue Jussieu, 75005 Paris, France

[2]Department of Earth Science, University of California, Santa Barbara 93106, USA

[3] CAS Key Laboratory of Crust-Mantle Materials and Environments, School of Earth and Space Sciences, University of Science and Technology of China, Hefei, Anhui 230026, China

[4]Nordic Volcanological Center, Institute of Earth Sciences, University of Iceland, Reykjavík, Iceland

[*] Corresponding author (email: bwang@ipgp.fr).

Abstract

Rubidium is a moderately volatile element with high incompatibility and fluid mobility. Its stable isotopes have great potential in tracing various geological processes. For example, lunar rocks are isotopically heavier than terrestrial ones, suggesting volatile loss by evaporation during or following the formation of the Moon. However, these studies rely on a poorly constrained estimate for the composition of the Earth's mantle and a poor understanding of high-temperature processes which may act to fractionate stable Rb isotopes. It is therefore important to precisely characterize different rock types that sample the Earth's mantle as well as to evaluate the importance of key isotopic fractionation processes. In order to address these issues, we established a high precision analytical method for Rb isotopic measurements using the Nu Sapphire CC-MC-ICP-MS (collision-cell multi-collector inductively coupled plasma mass spectrometer). In addition, we present a series of Rb isotopic data of volcanic rocks from Hekla volcano (Iceland) and MORB (mid-ocean ridge basalt) samples. We show that our method returns a high Rb sensitivity (~500 V/μg•g^{-1} for ^{85}Rb) and a long-term reproducibility of 0.03‰ on δ^{87}Rb (the permil deviation of the ^{87}Rb/^{85}Rb ratio from the SRM 984 standard). This method uses a 2 ng/g Rb solution for analyses, allowing us to consume about 10 times less Rb to achieve similar or better precision than previous studies. Using this method, seven geostandards and one synthetic standard return Rb isotopic data consistent with previous work. Twenty-one Hekla volcanic rocks, spanning compositions from basalt to rhyolite, show limited Rb isotopic variation, with δ^{87}Rb values varying from -0.17‰ to -0.07‰, demonstrating

that magmatic evolution has an insignificant effect on Rb isotope ratios. A set of MORB samples (n=15) from different mid-ocean ridges also span a limited Rb isotopic variation, displaying a range similar to the Hekla rock suite (-0.19 to -0.02‰). Combining our new data together with previously reported OIB data gives an average δ^{87}Rb value of -0.12 ± 0.08‰ (2SD, n=25), representing the current best estimate of the mantle's isotopic composition. Considering the δ^{87}Rb values of the upper continental crust (-0.14 ± 0.01‰, 2SE, n=73), as inferred from recent measurements of granites, loess and sediments, and assuming this value represents the whole crust, the revised Rb isotopic composition of the bulk silicate Earth (and by extension the bulk Earth, assuming no Rb partitioned into the core) is -0.13 ± 0.06‰ (2SD).

1. Introduction

Rubidium (Rb) is a univalent lithophile alkali metal element. Due to its high incompatibility, Rb is enriched in crustal materials compared to the mantle. The estimated Rb abundances of the lower, middle, and upper continental crust are 11 μg/g, 65 μg/g and 84 μg/g, respectively (Rudnick and Gao, 2003), while that in the primitive mantle is only 0.6 μg/g (McDonough and Sun., 1995), and the depleted upper mantle is 0.05 μg/g (Workman and Hart, 2005). Rubidium is a fluid-mobile element (Han et al., 2021; X. Hu et al., 2022) and it is moderately volatile with a 50% condensation temperature (T_c^{50}) of 800 K (Lodders, 2003). Similar to other moderately volatile elements (MVE) such as K, Cu, Zn, Cd, Cl, S and Se (Luck et al., 2005; Wombacher et al., 2008; Paniello et al. 2012; Boyce et al., 2015, 2018; Wing

and Farquhar, 2015; Pringle et al., 2017; Barnes et al., 2019; Tian et al., 2019, 2021; Gargano et al., 2020; Van Kooten et al., 2020; Vollstaedt et al., 2020; Y. Hu et al., 2022; Paquet et al. 2022), Rb stable isotopes show promise for studying mechanisms of volatile depletion processes in the inner Solar System.

Rubidium has two naturally occurring isotopes: the stable isotope ^{85}Rb (72.17%) and the radioactive isotope ^{87}Rb (27.83%) (Berglund and Wieser, 2011). However, ^{87}Rb is also considered as a stable isotope due to its long half-life (4.97×10^{10} y, where ^{87}Rb decays to ^{87}Sr) (Nebel et al., 2011b). Previous applications of Rb stable isotopes mainly focused on cosmochemical processes. For example, tektites were analyzed for Rb isotopes in order to explore the influence of impact melting (Nebel et al., 2005). Nebel et al. (2011a) reported Rb isotopic compositions of chondrites and observed resolvable variations on the order of ±1‰ δ^{87}Rb in some meteorites. Pringle and Moynier (2017) established a high-precision analytical method and reported Rb isotopic data of a series of terrestrial and extraterrestrial samples, including chondrites, achondrites and lunar samples. The results show significant Rb isotopic differences among these samples, especially lunar samples, which exhibit Rb isotopic compositions that are heavier than the Earth's mantle by ~ 0.2 permil. Subsequent measurements employing a different analytical method, have also found heavy Rb isotopic signatures in lunar rocks compared to terrestrial samples (Nie and Dauphas, 2019). All these studies show that Rb isotope can be used as a powerful tool to study planetary evolution.

However, these planetary studies rely on the Earth's mantle composition estimated by Pringle and Moynier (2017), and very few studies have applied Rb isotopes to terrestrial samples. Pringle and Moynier (2017) estimated the Rb isotopic composition of the mantle (δ^{87}Rb=-0.12 ± 0.06‰, 2SD) based on only 6 samples, including one mid-ocean ridge basalt (MORB) from the Atlantic ridge, two ocean island basalts (OIB) (Galapagos and Hawaii), one continental flood basalt (BCR-2), one andesite (AGV-2) and one granite (GS-N). X. Hu et al. (2022) constrained the composition of the upper continental crust (UCC) to be −0.14 ± 0.01‰ (2SE, n=73) based on an extensive sample set of granites, loess and sediments. A few additional igneous geostandards have also been analyzed for Rb stable isotopes (Zhang et al., 2018; Nie and Dauphas, 2019; Nie et al., 2021) (see Table 1).

Since the estimation of the Rb isotopic composition of the mantle is a key parameter for inter-planetary comparison, the limited set of data obtained from mantle-derived materials calls for a more comprehensive characterization. The very low Rb contents (~0.05 μg/g; Workman and Hart, 2005) makes it relatively difficult to directly analyze depleted peridotites (e.g., more than 200 mg of samples are needed with the highest sensitivity to date, i.e., 250 V/μg•g^{-1}, Pringle and Moynier, 2017). In this regard, MORBs are obvious targets as they are generated via partial melting of depleted upper mantle materials, thus providing a straightforward way to constrain the composition of this important reservoir, assuming no isotopic fractionation is generated during partial melting (Hofmann, 2003). Furthermore, magmatic evolution is known to fractionate stable isotopes of various isotopic systems (e.g., Fe, Teng et

al., 2008; Sn, Badullovich et al., 2017) and it is important to evaluate this effect on Rb isotopes. Previous Rb isotopic analyses of geostandards of different compositions found that Rb tends to become lighter gradually from mafic to felsic rocks (Zhang et al., 2018; Hu et al., 2021). These isotopic differences observed among the geostandards are relatively minor, typically within the range of approximately 0.2‰. This variability may also be attributed to the mantle source of the analyzed lavas. However, it is worth noting that geostandards are mass-produced and may become contaminated during production as suggested by studies of Mo isotopes (Willbold and Elliott 2017). Therefore, they may not be ideal for accurately estimating magmatic processes on Rb isotopes. In order to better determine the behavior of Rb isotopes during magmatic evolution, it is therefore necessary to investigate a co-genetic rock suite that is largely controlled by magmatic differentiation from a common parental melt. The Hekla volcano produced eruptive materials that range from basalt to rhyolite (Thorarinsson, 1967) and the Hekla suite has been used extensively in recent years to study isotopic fractionation during igneous processes responsible for formation of high-Si igneous rocks for various isotopic systems (e.g., Fe, Li, Schussler et al., 2009; Si, Savage et al., 2011; V, Prytulak et al., 2016; Zn, Chen et al., 2013; Tl, Prytulak et al., 2017; Ti, Deng et al., 2019; K, Tuller-Ross et al., 2019; Cl, Ranta et al., 2021; Ba, Bai et al., 2022). Hekla is, therefore, well suited for evaluating the behavior of Rb during igneous processes ultimately forming high-Si igneous rocks.

Here, we developed a new analytical method and report the first high precision Rb isotopic data using a Nu Sapphire CC-MC-ICP-MS (collision-cell multi-collector

inductively coupled plasma mass spectrometer). We present Rb isotopic compositions for a variety of samples, including 21 igneous rocks from Hekla volcano, and 15 MORBs from different mid-ocean ridge segments, as well as seven different igneous geostandards. Based on these data, we assess the effect of magmatic processes on Rb isotopes and estimate the average Rb isotopic composition of the mantle. Combining our findings from the mantle with the extensive crustal dataset previously reported by X. Hu et al. (2022), a more precise constraint on the Rb isotopic composition of the bulk silicate Earth (BSE) is provided in this study.

2. Samples

2.1. Geostandards

In order to test the accuracy of our new method, a number of geostandards with compositions ranging from basalt to granite were selected because they have previously been analyzed for their Rb isotopic compositions. The geostandards comprise BHVO-2 (basalt, United States Geological Survey, USGS), BCR-2 (basalt, USGS), W-2a (diabase, USGS), AGV-2 (andesite, USGS), GSP-2 (granodiorite, USGS), GS-N (granite, Centre de Recherches Pétrographiques et Géochimiques, CRPG), and GA (granite, CRPG). We also mixed pure NIST SRM 984 solution (the Rb isotopic standard) with PCC-1 (peridotite, USGS) to be treated as a synthetic standard to evaluate the accuracy of the measurements.

2.2. Hekla volcano samples

In recent years, the Hekla magma suite has been extensively utilized for investigating isotopic fractionation during magmatic processes (e.g., Savage et al., 2011; Chen et al., 2013; Prytulak et al., 2017; Deng et al., 2019; Tuller-Ross et al., 2019). A set of Hekla volcanic rocks were collected (see sample locations in Bai et al., 2022) and analyzed for Rb isotope in this study. Located at the margin of the propagating South Iceland Volcanic Zone, Hekla volcano is an active central volcano in Iceland that rises nearly 1500 masl (meters above the sea level; Thorarinsson, 1967). It is well-known as a natural laboratory for investigating magmatic processes and the origin of high-Si rocks (Sigmarsson et al., 1992, 2022; Geist et al., 2021). It erupts a series of cogenetic volcanic products, including basalts, basaltic andesites, andesites, dacites and rhyolites. At present, origin of Hekla's wide compositional variability is a matter of debate. Sigmarsson et al. (1992) proposed a three-stage model to explain generation of Hekla's igneous rocks from basalt to rhyolite: (1) The rise of basaltic magma causes partial melting of metabasaltic crust, thus forming dacitic magma. (2) The basaltic magmas undergo fractional crystallization to generate basaltic andesite compositions, and the latter mixes with dacitic liquid to form andesites. (3) Rhyolites are formed from dacitic magma through fractional crystallization. Chekol et al. (2011) suggested that andesitic to more evolved compositions were produced through AFC (assimilation and fractional crystallisation) processes. These studies both advocated the contribution of crustal components to high-Si rocks (i.e., assimilation and/or partial melting of the crust). By contrast, Geist et al. (2021) suggested that the entire Hekla suite is formed by fractional

crystallization processes alone, over a period of several tens of thousands of years. A more recent study argued that partial melting of the metabasaltic crust remains the preferred mechanism for petrogenesis of the Hekla silicic rocks, with the time span from silicic magma formation to eruption being less than a few centuries (Sigmarsson et al., 2022).

In this study, we analyzed 9 basalts, 6 basaltic andesites, 2 andesites, 3 dacites and 1 rhyolite from Hekla volcano. Some of these have previously been analyzed for their Ba isotopic composition (Bai et al., 2022). The Hekla rocks studied here are generally fresh, Holocene igneous rocks with little to no visible signs of secondary alteration (Sigmarsson et al., 1992; Chekol et al., 2011; Geist et al., 2021). Furthermore, besides some rare secondary incrustations, formed during solidification, cooling and secondary degassing (Óskarsson, 1981), the vast amount of data published from the Hekla suite does not indicate that secondary alteration affects the chemical and isotopic composition. Thus, the Hekla suite records extensive magmatic evolution of a OIB magma, from basalt through rhyolite, making this suite ideal for studying the effect of magmatic processes on Rb isotopes.

2.3. MORB samples

Sixteen MORB samples from different mid-ocean ridge segments were collected to estimate the Rb isotopic composition of the upper mantle. Among them, nine are from the Atlantic Ocean, four are from the Indian Ocean and three are from the East Pacific Ocean. All MORB samples in this study are fresh glasses (quenched melts), which were not subjected to significant alteration as indicated by the chemical index

of alteration (CIA) and loss on ignition (LOI) (She et al., 2023). According to a common classification scheme (Schilling, 1975; Schilling et al., 1983), MORB samples can be divided into Normal-MORBs (N-MORBs, $La/Sm_N<0.7$), Enriched-MORBs (E-MORBs, $La/Sm_N > 1.8$) and Transitional-MORBs (T-MORBs, with La/Sm_N between N- and E-MORBs). Importantly for the purpose of this study, these MORB samples cover all the different types mentioned above (Amsellem et al., 2018; Deng et al., 2018; Inglis et al., 2019), which allows us to evaluate the role of partial melting and/or mantle source-derived variability on $\delta^{87}Rb$ values.

3. Analytical methods

3.1. Sample dissolution

Sample digestion and chemical purification were conducted at the Institut de Physique du Globe de Paris (IPGP). 18.2 MΩ·cm ultrapure water and distilled high-purity concentrated acids were used throughout the processes. For each Hekla sample, whole-rock powder was made from approximatively 50g of rock. For MORB samples, fresh glass fragments were handpicked and powdered with an agate mortar (She et al., 2023). 20-60 mg of sample powders were weighed into Savillex PFA Teflon beakers to yield >10 ng Rb for isotopic measurement. A separate 50 mg of Hekla sample powders were weighed for major and trace elements measurement. Samples were first digested with a 3:1 volume mix of concentrated HF and HNO_3 by heating at 130 °C for 48h on a hotplate. After evaporation of HF-HNO_3, the samples were sequentially treated with aqua regia (concentrated HCl: HNO_3=3:1, volume ratio) and 6 mol/L HCl

at 120 °C to remove fluoride complexes. Finally, dried samples were re-dissolved in 1 mL 0.5 mol/L HNO_3 for major and trace elements measurements, or re-dissolved in 1 mol/L HNO_3 for subsequent column chemistry.

3.2. Major and trace elements measurement

Full basic geochemical data of the MORB samples has been reported in She et al. (2023). Elemental concentration measurement was performed for all the Hekla samples at IPGP. An aliquot of the digested solution was diluted by a factor of 15000 for elemental analysis. Major and trace elements were measured using an Agilent quadrupole inductively coupled plasma mass spectrometer (Q-ICP-MS). Two geostandards (i.e, BHVO-2 and BCR-2) were processed with the same procedures to monitor the accuracy. The data are provided in the Supplementary Material.

3.3. Chemical purification and Rb isotopic measurement

Pringle and Moynier (2017) developed a column chemistry procedure of Rb isotopes at IPGP. The procedure consists of four steps, with one column of Eichrom DGA resin (50–100 μm, 1.8 mL) to remove Ca, then two columns of Bio-Rad AG50W-X12 resin (200–400 mesh, 20 mL and 10 mL, respectively) to remove other matrix elements, and finally one column of Bio-Rad AG50W-X8 resin (200–400 mesh, 1 mL) to further separate K. However, this procedure is time-consuming and requires large volumes of acid. Previous studies showed that the separation of Rb and K could be successfully realized by using Sr-spec resin (Zhang et al., 2018; Nie and Dauphas, 2019; Hu et al., 2021). Thus, based on the column chemistry established by Pringle and Moynier (2017), we modified the last step by replacing it with a Sr-spec resin

chemistry. The full chemical purification procedure is listed in Supplementary Table 1, in which the first three steps have been described in Pringle and Moynier (2017) and remain the same here. In the text that follows, we provide a detailed description of only the last step (i.e., Sr-spec purification).

After the first three steps of purification, sample elution was dried down and re-dissolved in 3 mol/L HNO_3 for Sr-spec column chemistry. 1 mL Eichrom Sr-spec resin (25–50 μm) was filled into a pre-cleaned homemade heat-shrink Teflon column (0.46 cm inner diameter, 6.5 cm length). The resin was cleaned with 3 mL of 3 mol/L HNO_3 and 2 mL of H_2O successively, and then conditioned with 3 mL 3 mol/L HNO_3 prior to sample loading. Sample was loaded on the resin in 0.25 mL of 3 mol/L HNO_3 and followed by another 0.25 mL of 3 mol/L HNO_3. The Rb was collected with 1 mL 3 mol/L HNO_3 (Supplementary Table 1). Compared to the AG50W-X8 resin method (which required 40 mL of acid to collect Rb) that was previously used by Pringle and Moynier (2017), the Sr-spec in this study used only 1 mL of acid. This greatly simplifies the chemical purification process. Using the Sr-spec method, we can achieve a complete separation of Rb from K (Fig. 1).

The recovery and blank of the whole procedure were carefully evaluated. The yield of each sample was >95%, and the total procedural blank was <0.03 ng, which was negligible (<0.3%) compared to the total Rb in sample (>10 ng).

Rubidium isotopic measurements were performed on CC-MC-ICP-MS Nu Sapphire at IPGP. The Nu Sapphire is a new generation double-focusing MC-ICP-MS which includes both a high energy ion pathway (traditional MC-ICP-MS) and a low

energy ion pathway (equipped with a collision cell). For Rb isotopic measurements, we used conventional high energy mode. Sample solution was introduced through an Apex Omega desolvating system using a 100 μL/min PFA nebulizer (Elemental Scientific, Omaha, NE, USA). Rubidium isotopic abundances were analyzed in low resolution mode with standard Ni dry cones ("dry plasma"). The isotopes ^{85}Rb and ^{87}Rb were simultaneously collected on L3 and H1 Faraday cups, respectively, with $10^{11}\Omega$ resistors, respectively. Strontium-88 was collected on the H3 Faraday cup ($10^{11}\Omega$ resistor) in order to evaluate ^{87}Sr intensity. The interference of ^{87}Sr on ^{87}Rb is corrected by assuming an $^{87}Sr/^{88}Sr$ value of 0.085, following prior work (Nebel et al., 2005; Pringle and Moynier, 2017; Zhang et al., 2018; Hu et al., 2021). A constant $^{87}Sr/^{88}Sr$ ratio of 0.085 is sufficient for the Sr correction, because the ^{87}Sr interference on ^{87}Rb is insignificant due to efficient Sr removal during column chemistry, and thus the uncertainty on the $^{87}Sr/^{88}Sr$ ratio would have a minor impact. For example, taking two extreme values of $^{87}Sr/^{88}Sr$ (0.083 and 0.089, corresponding to $^{87}Sr/^{86}Sr$ of 0.70 and 0.75, respectively) from the reported range in terrestrial and extraterrestrial rocks and for the sample with the most Sr residue ($^{88}Sr/^{85}Rb$=0.003), would only affect the correction by only ~ 0.03‰.

Relevant operating parameters of the instrument are shown in Supplementary Table 2. The sensitivity of ^{85}Rb was ~500 V/μg•g^{-1}. Samples and standard solutions were diluted to 2 ng/g using 0.5 mol/L HNO_3 for analyses. Before each analysis, a 30-second blank measurement was performed in 0.5 mol/L HNO_3. Each sample analysis consisted of 40 cycles of data with an integration time of 5 seconds per cycle. In order

to eliminate potential cross-contamination, the sample introduction system was cleaned 90 seconds using 0.5 mol/L HNO_3 following each standard and sample analysis. Each sample was measured at least 3 times, bracketed by the international isotopic standard NIST SRM 984. Rubidium isotopic data were reported as $\delta^{87}Rb = [(^{87}Rb/^{85}Rb)_{sample} / (^{87}Rb/^{85}Rb)_{SRM984} - 1] \times 1000$ (‰).

4. Results

The pure NIST SRM 984 solution yielded $\delta^{87}Rb$ values between -0.05‰ and +0.04‰, with an average of 0.00 ± 0.03‰ (2SD, n=23; Fig. 2a and Supplementary Table 4). Rubidium isotopic compositions of one in-house standard (IPGP-Rb, a pure Rb ICP-MS solution), previously used in Pringle and Moynier (2017) and seven geostandards are presented in Table 1, and literature values are also listed for reference. The value of IPGP-Rb (-0.12 ± 0.02‰, 2SD, n=6) was identical to that (-0.12 ± 0.08‰, 2SD, n=40) measured by Pringle and Moynier (2017) using a Thermo-Fisher Neptune plus. The $\delta^{87}Rb$ values of geostandards all agree well with previously published data (Fig. 2b). In addition, some of these geostandards are used to test the effect of the measuring concentrations (Fig. 3). These results are discussed in section 5.1.

Hekla samples data are reported in Table 2. Consistent with previous studies (e.g., Sigmarsson et al., 1992, 2022; Geist et al., 2021), Rb contents of Hekla suite display reasonably good correlations with SiO_2 and MgO contents as well as other incompatible minor (K_2O) and trace elements (La), gradually increasing with the

magmatic evolution (Fig. 6a, b, c and d), which is consistent with its strong incompatibility. The average Rb concentrations of these five rock types—basalts, basaltic andesites, andesites, dacites, and rhyolite—are 10.4 μg/g, 27.2 μg/g, 29.2 μg/g, 55.7 μg/g and 68.3 μg/g, respectively. However, irrespective of Rb contents, all Hekla samples show uniform Rb isotopic composition within uncertainty, with δ^{87}Rb values ranging from -0.17 to -0.07‰ (Fig. 6e and f).

The $(La/Sm)_N$ of MORB samples ranges from 0.4 to 2.0 (Table 3 and Fig. 7a), covering different types of N-MORB, E-MORB and T-MORB (Schilling, 1975; Schilling et al., 1983). Rubidium isotopic compositions of MORBs vary from -0.19 to -0.02‰, with an average of -0.12 ± 0.09‰ (2SD, n=15). Most of the different types of MORB samples exhibit similar Rb isotope signatures, except one E-MORB sample (CH30 DR 17-03), which has slightly heavier Rb isotopic composition (-0.02 ± 0.02‰, 2SD) than others (Fig. 7a and b). Nevertheless, Rb isotope data of MORB samples in this study shows no obvious trend with Rb and MgO contents, Na_8 and Ba/Th (Fig. 7b, c, d and e).

5. Discussion

5.1. Validating high precision Rb isotopic measurements using a Nu Sapphire

5.1.1 Accuracy and precision

In order to evaluate the accuracy of our method, we first analyzed the pure NIST SRM 984 solution. Self-bracketing NIST SRM 984 solutions generated the expected δ^{87}Rb values around zero (within the uncertainty), with an average of 0.00 ± 0.03‰

(2SD, n=23; Fig. 2a). In addition, a synthetic sample (SRM 984+PCC-1, after Rb separation following column chemistry) was also measured to test the matrix separation efficiency of the chemical purification. This peridotite sample, PCC-1 contains almost no Rb (0.07 μg/g, Takazawa et al., 2000; Sossi et al., 2016). Approximately 20 mg of PCC-1 powder was digested and then redissolved into 1mL of pure SRM 984 solution which contained 25 ng of Rb. Given the mass ratio of Rb contained in SRM 984 and PCC-1 (i.e., 25:1.4), 95% of the Rb of this synthetic sample comes from the pure SRM 984. Due to its low Rb content, the Rb isotopic composition of PCC-1 has never been measured, but assuming that its δ^{87}Rb value is within ± 1 ‰ from SRM 984 (this is reasonable because as a peridotite it should have Rb isotopic characteristics comparable to that of the mantle, i.e., δ^{87}Rb=-0.12 ± 0.06‰, 2SD; Pringle and Moynier, 2017), this synthetic sample should have isotopic composition that is within error of the pure SRM 984 after column chemistry. The results obtained validate this prediction because the average δ^{87}Rb value of the three synthetic samples is -0.01 ± 0.03‰ (2SD, n=3). This confirms the reliability of matrix separation of our chemistry. The in-house standard IPGP-Rb solution and seven geostandards were analyzed to further test the accuracy of our method (Fig. 2b). All the results presented in this study are consistent with previously published data (Pringle and Moynier, 2017; Zhang et al., 2018; Nie and Dauphas, 2019; Nie et al., 2021; Hu et al., 2021). The long-term reproducibility of our Rb isotopic analyses is 0.03‰ (2SD), as estimated from the repeated measurements of AGV-2 (δ^{87}Rb=-0.14 ± 0.03‰, 2SD, n=17; Fig. 2a and Supplementary Table 4) during 17 analytical

sessions over 3 months (where, in each session, AGV-2 was measured at least 3 times).

5.1.2 Effect of Rb concentration

The Nu sapphire coupled to the Apex Omega allows us to obtain the highest sensitivity (500 V/μg•g^{-1} for ^{85}Rb) ever achieved compared with previous studies, e.g., 100 to ~250 V/μg•g^{-1} in Pringle and Moynier (2017), 50 V/μg•g^{-1} in Zhang et al. (2018) and Nie et al. (2021), and 45 V/μg•g^{-1} in Hu et al. (2021). For the purposes of evaluating the effect of measuring concentrations on accuracy and precision, and examining the lower limit of the analytical concentration on the Nu Sapphire, we measured IPGP-Rb, BHVO-2, GSP-2, and AGV-2 at various Rb concentrations. The concentrations of samples and bracketing standards were set from 10 ng/g, 2 ng/g, 1 ng/g and even 0.5 ng/g. Under different conditions, even if the Rb concentration was as low as 0.5 ng/g, we could obtain accurate values consistent with previously reported data for these standards. However, the analytical precision decreases significantly at the lowest running concentrations. For example, the precisions reported for 10 ng/g and 2 ng/g are within 0.05‰ (2SD), but precision is generally worse and more variable at 1 ng/g (down to 0.14‰, 2SD). At 0.5 ng/g the precision is 0.38‰ (2SD) (Fig. 3 and Supplementary Table 5). Given that at 2 ng/g measurements still provide excellent precision, we set 2 ng/g as the analytical concentration for the rest of this work. This allows us to perform Rb isotopic measurement with only a small amount of sample.

5.1.3 Effects of concentration and acid molarity mismatch

Previous studies demonstrated that a concentration mismatch between standards

and samples can have a more significant impact on measurements of K, Ca and Cu isotopes on the Nu Sapphire compared to Neptune or Neptune Plus, and an intensity match within 1% was suggested during analysis (Moynier et al., 2021; Dai et al., 2021; Wang et al., 2022). In order to test the effect of concentration mismatch on Rb isotopic measurements, pure SRM 984 solutions with different Rb concentrations were analyzed as unknown samples. The bracketing standard was kept at 10 ng/g, while samples were run with concentrations varying from ~5 ng/g to 15 ng/g (i.e., the ratio of sample/standard varied from just under 0.5 to a bit over 1.5). Unlike K and Ca isotopes, Rb isotopic analyses on Nu Sapphire are insensitive to the concentration mismatch (Fig. 4a and Supplementary Table 6)

It was also reported that Nu Sapphire measurements may be more sensitive to mismatch of acid molarity between samples and bracketing standard (Moynier et al., 2021; Dai et al., 2021; Chen et al., 2021; Li et al., 2022; Wang et al., 2022; Zheng et al., 2022). The influence of acid molarity mismatch on Rb isotopic measurements was assessed by a series of condition tests. Pure SRM 984 solutions were treated as samples, and measured with the same Rb concentration (i.e., 2 ng/g) as the bracketing standard. However, they were prepared with different molarities of acid. The standard was diluted using 0.5 mol/L HNO_3, while samples were diluted in HNO_3 at various concentrations (from 0.1 mol/L to 1.0 mol/L). The results show that acid molarity mismatch has no obvious effect on the Rb isotopic measurements when analyzed on the Nu Sapphire (Fig. 4b and Supplementary Table 6). Nevertheless, we use the same HNO_3 (0.5 mol/L) to prepare samples and standard solutions during measurements.

5.1.4 Effect of matrix elements

A small amount of matrix residues after column chemistry may also influence isotope measurements. For example, interferences of isobars and polyatomic ions, and influences of matrix on ionization and transmission of target elements, can affect the quality of the isotopic measurements (Tan and Horlick, 1987; Tanner, 1992; Chen et al., 2021). In particular, previous studies have reported that some matrix elements can strongly affect Rb isotopic values during mass spectrometry analysis (Zhang et al., 2018; Nie and Dauphas, 2019; Hu et al., 2021). In this study, we tested these effects on the Nu Sapphire, of Sr, K, Cr, Ga, Ca, Ti, Fe, Mn, Al and Na. Pure standard solutions of various elements were doped into a 2 ng/g SRM 984 to obtain different ratios of [element]/[Rb]. The doped solutions were measured against pure SRM 984 with the same Rb concentration. The results are presented in Fig. 5 and Supplementary Table 7.

Strontium correction with a fixed $^{87}Sr/^{88}Sr$ value of 0.085 is effective only when there is a very small amount of Sr residue in the Rb solution. The result of our Sr doping test showed that accurate $\delta^{87}Rb$ values could be obtained when $Sr/Rb \leq 0.005$ (i.e., $^{88}Sr/^{85}Rb$ intensity ≤ 0.006). In order to minimize the impact of the isobaric interference of ^{87}Sr on ^{87}Rb, all natural samples in this study had $^{88}Sr/^{85}Rb$ intensity $\leq$ 0.003 (for most samples the ratio was ≤ 0.002 or lower) after chemical purification, and therefore the Sr correction did not affect the quality of the $\delta^{87}Rb$ data. Because Rb and K have very similar geochemical behavior, a challenge of our method is to achieve complete separation of Rb and K. Previous studies have shown that K affects Rb isotopic measurements, but to different degrees between different instruments. For

example, Pringle and Moynier (2017) (Neptune Plus with quartz cyclonic spray chamber or Apex) and Zhang et al. (2018) (Neptune Plus with quartz dual cyclonic-Scott spray chamber) found that the K/Rb ratios must be maintained below 10 and 25, respectively, to obtain accurate δ^{87}Rb values. Nie and Dauphas (2019) (Neptune with quartz dual cyclonic-Scott spray chamber) found that it was sufficient to keep it below 50. A more recent study found that the isotopic measurements were very sensitive to K residue (Neptune Plus with quartz dual cyclonic-Scott spray chamber; Hu et al.,2021) with the δ^{87}Rb values shifted when K/Rb $>$ 1.5. Thus, it is necessary to evaluate the effect of K on Rb isotopic measurements on the Nu Sapphire coupled to an Apex Omega. Our doping test results showed that Rb isotopic analyses were not affected by K as long as the K/Rb ratio $\leq$ 20. Chromium and Ga were doped here to test the effect of some possible impurities, since they are eluted very closely to Rb according to the elution curves presented in Pringle and Moynier (2017). The influence was negligible as long as Cr/Rb was $\leq$ 10 and Ga/Rb was $\leq$ 20. Other matrix elements (such as Ca, Ti, Fe, Mn, Al and Na) affected Rb isotopic measurements to different extent. δ^{87}Rb values were modified when Ti/Rb was $\geq$ 20, Fe/Rb was $\geq$ 20 and Al/Rb was $\geq$ 10, while Ca, Na and Mn had no obvious influence within the range of concentration ratios set in our doping tests (i.e., [element]/[Rb] $\leq$ 50).

5.2. Magmatic processes do not fractionate Rb isotopes

Igneous products of the Hekla volcano have been widely used to investigate behaviors of different isotopic systems during magmatic processes. For example, Th, Fe, Si, B and V isotopic compositions of Hekla igneous rocks correlate with SiO_2

contents, suggesting that magmatic evolution has a significant influence on these isotope systems (Sigmarsson et al., 1992; Rose-Koga and Sigmarsson, 2008; Schuessler et al., 2009; Prytulak et al., 2016; Savage et al., 2011). Moreover, highly light Cl isotopic values observed in high-Si rocks from Hekla have been interpreted to reflect the assimilation of magmatic brine (Ranta et al., 2021). However, no isotopic variation was observed in the same set of samples for Li, Zn, Mo, Tl, K and Ba isotopes (Schuessler et al., 2009; Chen et al., 2013; Yang et al., 2015; Prytulak et al., 2017; Tuller-Ross et al., 2019; Bai et al., 2022). A set of igneous rocks from the Hekla volcano were analyzed in this study in order to explore the Rb isotopic behaviors during magmatic evolution. In the following sections, we will systematically evaluate different magmatic processes which have the potential to fractionate Rb isotopes.

5.2.1 Assimilation and/or exsolution of magmatic fluids

As Rb is a fluid-mobile element, hydrothermal fluid activities may lead to its isotopic fractionation. For example, X. Hu et al. (2022) reported a highly heavy Rb isotopic signature (-0.29‰ to 1.20‰) in Kampa leucogranites compared to the available data on sedimentary materials of the UCC (-0.31‰ to 0.07‰). After ruling out the influences of source heterogeneity, partial melting, fractional crystallization and chemical weathering, this highly heavy Rb isotopic signature was attributed to the involvement of magmatic fluids (X. Hu et al., 2022). This is consistent with previous studies that have also shown that Kampa leucogranite magma was modified by fluids during its evolution (Liu et al., 2020; Huang et al., 2021). Therefore, the influence of assimilation and/or exsolution of magmatic fluids need to be considered.

Previous chlorine isotopes study indicates that the assimilation of magmatic brine plays an important role in generating light chlorine isotopic characteristics evident in Hekla rhyolites (Ranta et al., 2021). However, we do not observe any abnormal signals in high-Si rocks from Hekla, either in terms of Rb concentration or isotopic composition. For example, Rb contents follow a consistent evolution trend when plotted against SiO_2 and MgO contents (Fig. 6a and b). Besides, compared with associated basalts ($\delta^{87}Rb_{average}$= -0.12 ± 0.06‰, 2SD, n=8) and basaltic andesites ($\delta^{87}Rb_{average}$= -0.15 ± 0.06‰, 2SD, n=6), dacites ($\delta^{87}Rb_{average}$= -0.15 ± 0.03‰, 2SD, n=3) and one rhyolite sample ($\delta^{87}Rb$= -0.17 ± 0.04‰) have similar Rb isotopic compositions. This similarity indicates that the influence of magmatic brine on Rb isotope in our samples is not obvious, if indeed magmatic brines are concentrated in rhyolites relative to basalts and dacites. In addition, fluid exsolution is also unlikely to affect Rb isotopic signature of Hekla rocks, given the identical Li isotopic composition of the different Hekla lavas, which indicates that exsolution of fluids from melt is not significant (Schuessler et al., 2009).

5.2.2 Degassing

Rubidium is a moderately volatile element with a T_c^{50} of 800 K (Lodders, 2003). Previous studies on extraterrestrial samples indicate that volatile loss during evaporation may lead to Rb isotopic fractionation (Pringle and Moynier, 2017; Nie and Dauphas, 2019). Hekla lavas experience significant loss of F, Cl and S during eruptions (Moune et al., 2007; Ranta, et al., 2021). Therefore, Rb isotope fractionation caused by volatile loss during volcanic degassing is possible.

While the Rb isotopic compositions of Hekla rocks are relatively uniform and non-systematic, the total variation observed (~0.10‰) exceeds the precision of our method (0.03‰). Rubidium isotopes can therefore be used to estimate the amount of Rb loss during volcanic degassing at Hekla. Rubidium is evaporated as RbCl gas during degassing, and the theoretical Rayleigh fractionation coefficient (α) can be calculated as the square root of the mass difference between ^{85}RbCl and ^{87}RbCl [i.e., $(120.3648/122.3622)^{0.5} = 0.9838$]. Based on this, we can estimate a maximum of 0.6% of Rb is lost during volcanic degassing, which is similar to the loss amount of K (0.8~1.3%) estimated by Tuller-Ross et al. (2019). However, it should be noted that this estimation is based on the assumption that the Rb isotopic variation of Hekla rocks is entirely due to degassing. As a result, the actual loss of Rb during volcanic degassing may be much less than our estimated value. This is supported by the fact that the Rb contents are consistent with the behavior of other non-volatile incompatible elements (e.g., La) during magma evolution (Fig. 6d), indicating that there may be no significant loss of Rb following magma evolution at Hekla. Therefore, we conclude that volatile loss associated with petrogenesis of the Hekla rock suite is unlikely to fractionate Rb isotopes.

5.2.3 **Magmatic evolution**

The Hekla basaltic to intermediate rocks are commonly considered to be controlled by fractional crystallization process (Sigmarsson et al., 1992, 2022; Geist et al., 2021). Currently, there is an ongoing debate regarding the petrogenesis of the silicic rocks from Hekla. For example, studies of short-lived radiogenic isotopes

(Sigmarsson et al., 1992, 2022; Chekol et al., 2011) and B and Cl stable isotopes (Rose-Koga and Sigmarsson, 2008; Ranta et al., 2021) suggest that crustal anatexis and assimilation are important processes for the formation of dacites, from which rhyolites are generated via fractional crystallization. Geist et al. (2021) suggested a "fractional crystallization alone" model, arguing that the evolution of magma at Hekla was primally driven by fractionation crystallization based on trends in trace element ratios, as well as oxygen isotopic data, with which they excluded significant contribution from the crust. The Hekla dacites, together with other types of rocks, show a good correlation between their Rb concentrations and SiO_2 as well as MgO contents, strictly following a magmatic differentiation trend (Fig. 6a and b). However, an influence of the crust cannot be ruled out, as partial melting of metabasaltic crust to form dacites also fits the consistent trend of elemental Rb. For example, we can roughly evaluate the contribution of the crust melting by using the equation: $C_1/C_0=F^{(D-1)}$, where C_1 is the Rb content of the melt (i.e., dacites), C_0 is Rb content of parent material (i.e., metabasalts), F is the degree of partial melting, and D is bulk partition coefficient of Rb. Using the average Rb concentration of dacites (54.8 μg/g) and basalts (10.5 μg/g) to represent C_1 and C_0 respectively. And assuming that the distribution coefficient of Rb during partial melting of the metabasalts is between 0 and 0.2 (which is the highest Rb partitioning of the dominant phenocryst phases in Hekla rocks according to Geist et al., 2021), it is estimated that the dacites can be formed by 13% to 19% partial melting of metabasalts. This is consistent with previous

505 estimates using elemental Th and U (10~20%, Sigmarsson et al., 1992, 2022) as well
506 as Tl (16%, Prytulak et al., 2017).

507 In cases where traditional major and trace elements analyses fail to distinguish
508 between competing petrogenesis models, emerging isotope systems may hold
509 potential for providing new insights. Therefore, we aim to investigate whether Rb
510 isotopes can offer new insights into the ongoing debate over the petrogenesis of Hekla.
511 The anhydrous phenocryst assemblage of Hekla lavas is dominated by plagioclase,
512 olivine, clinopyroxene, orthopyroxene, magnetite, apatite, ilmenite and zircon
513 (Sigmarsson et al., 1992, 2022; Geist et al., 2021). Based on partition coefficients
514 from Geist et al. (2021), we anticipate that only a limited amount of Rb would enter
515 these phases during fractional crystallization. This is consistent with what is observed
516 for K (Tuller-Ross et al., 2019). Since Rb and K are both highly incompatible
517 elements and the concentration of these elements correlate in the Hekla samples (Fig.
518 6c), they must exhibit very similar geochemical behavior during magmatic evolution.
519 Tuller-Ross et al. (2019) proposed that K-bearing minerals were absent when solid
520 phases crystallized from melt at Hekla. Rubidium mainly exists in the form of
521 isomorphic substitution of K, thus Rb would not get incorporated into solid phases
522 during magmatic evolution. This is also supported by the good correlation between Rb
523 and La (Fig. 6d) as well as other trace elements such as Tl, Ba, U, Th and Pb
524 (Sigmarsson et al., 1992; Prytulak et al., 2017; Geist et al., 2021). If considering that
525 the Hekla system undergoes fractional crystallization alone as proposed by Geist et al.
526 (2021), the magmatic process would not lead to significant Rb isotopic fractionation,

given that limited Rb enters the solid phases during fractional crystallization. For comparison, we also evaluate the impact in the case of crustal involvement during magmatic evolution. Prytulak et al. (2017) suggested that the contributions of crustal components were highly unlikely to be low temperature altered crust, pelagic clays and/or Fe-Mn sediments, based on the homogeneity of the Tl isotopic compositions across the range of magmatic products at Hekla. A recent study shows that the Rb isotopic composition of the upper continental crust (-0.14 ± 0.01‰, 2SE, n=73; X. Hu et al., 2022) is close to the mantle's composition (-0.12± 0.06‰, 2SD, n=6; Pringle and Moynier., 2017). The possible similarity of the Rb isotopic composition between the crust and mantle implies that even if the origin of dacites is influenced by the crustal contribution, they still have the same Rb isotopic composition as less evolved rocks. The two competing models (i.e., assimilation and/or partial melting of the crust versus fractional crystallization alone, Sigmarsson et al., 1992, 2022; Chekol et al., 2011; Geist et al., 2021), accordingly, both agree with the absence of resolvable Rb isotopic variation between the dacites ($\delta^{87}Rb_{average}$= -0.15 ± 0.03‰, 2SD, n=3) and other less evolved rock types (average δ^{87}Rb value of -0.12 ± 0.06‰, 2SD, n=8 for basalts and -0.15 ± 0.06‰, 2SD, n=6 for basaltic andesites). Therefore, the ongoing petrogenesis debate is not resolved with Rb isotopes.

The origin of dacites is still controversial. However, despite this uncertainty, the uniformity of δ^{87}Rb values in the Hekla rock suite suggests that magmatic processes do not significantly modify the Rb isotopic characteristics of the source melt. This is consistent with the prediction made by Zeng et al. (2019) through first-principle

calculations. They estimated that the Rb isotopic equilibrium fractionation between silicate melt and mineral would not exceed 0.01‰ at 900~1000℃, which is within our analytical uncertainty. It is, however, worth noting that Hekla is an anhydrous, tholeiitic system, and the behavior for Rb isotope could be different if a hydrous (e.g., biotite) or K-rich phases are involved during magma evolution.

5.3. Rubidium isotopic composition of the Earth's mantle

Magma emplaced at mid-ocean ridges makes up a major part of terrestrial magma production (White and Klein, 2014; Nan et al., 2022; Wu et al., 2023). MORBs are generated by partial melting of the mantle (Hofmann, 2003; White and Klein, 2014). According to Workman and Hart (2005), the bulk distribution coefficient $D_{solid/melt}$ of Rb during mantle partial melting can be low as 0.00001, and MORBs correspond to melting degrees between 6% and 20%. This means that during the partial melting of the mantle, more than 99% of Rb tends to enter the basaltic melt, and therefore we can safely assume that Rb isotopic fractionation does not occur during partial melting. The lack of correlation between Rb isotopic compositions and the indicator of partial melting degree Na_8 (which is defined as $Na_8=Na_2O + 0.373 \times MgO - 2.98$; Klein and Langmuir, 1987) of MORB samples in this study (Fig. 7d) is consistent with this assumption. In addition, Rb isotopic fractionation is very limited during magmatic evolution based on no obvious correlation between $\delta^{87}Rb$ and MgO contents (Fig. 7c) as well as our observation of Hekla volcanic rocks. Therefore, the Rb isotopic characteristics of MORB samples can reflect the composition of their mantle source.

In this study, various MORB samples with a broad geographical distribution were analyzed for Rb isotopes. All but one of these samples span a limited range of Rb isotopic compositions (-0.19 to -0.07‰) despite different localities. One exception is the E-MORB sample, CH30 DR 17-03, which is found to have a slightly heavier Rb isotopic composition (δ^{87}Rb=-0.02 ± 0.02‰, Table 3 and Fig. 7a). Previous studies proposed that formation of E-MORBs may be related to the involvement of deep recycling of crustal materials (Hofmann, 2003; Elliott et al., 2006). Although a recent study estimated the Rb isotopic composition of the upper continental crust is -0.14 ± 0.01‰ (2SE, n=73; X. Hu et al., 2022), low temperature alteration process would lead to significant Rb isotopic fractionation (Zhang et al., 2021) thus surface sediments or altered oceanic crust (AOC) may have abnormal Rb isotopic characteristics. Recycling of these materials may cause the inhomogeneity of the local mantle sources of MORBs. This may account for the heavier Rb isotopic characteristic associated with higher Rb content observed in CH30 DR 17-03 (Fig. 7b). However, the addition of abnormal Rb was unlikely via fluid, since extremely high Ba/Th, an indicator of fluid enrichment, is not observed in CH30 DR 17-03 (Fig. 7e). It is therefore, necessary to further test if Rb isotopes can be used to trace subduction recycling into the mantle, for example by targeting altered oceanic crust or sediments. In addition, it is worth noting that N-MORBs show more scattered Rb isotopic compositions compared to T-MORBs (Fig. 7a). A similar scatter for Sn isotopes was also observed in this set of samples (She et al., 2023). The scatter was unlikely caused by secondary modification, as the MORBs in this study did not undergo significant alteration

according to the CIA and LOI values (She et al., 2023). Thus, it is more likely related to the diversity of sampling sites as suggested by She et al. (2023), which span locations as diverse as the Atlantic, Indian, and East Pacific Ocean. Nevertheless, Rb isotopic compositions of all MORB samples cluster within a narrow range. Based on the average δ^{87}Rb value of these MORBs, the Rb isotopic composition of the upper mantle is estimated at -0.12 ± 0.09‰ (2SD, n=15). This value is consistent with the previous estimate (-0.12 ± 0.06‰, 2SD; n=6) from Pringle and Moynier (2017). If we assume that Rb isotopic compositions of OIBs also reflect the characteristics of their mantle source, we can combine MORBs and Hekla basalts in this study with the OIB data reported in the literature (Pringle and Moynier, 2017) to estimate the Rb isotopic composition of the mantle. This compilation yields a δ^{87}Rb value = -0.12 ± 0.08‰ (2SD, n=25; Fig. 8).

5.4. Rubidium isotopic composition of the Bulk Silicate Earth

As mentioned above, Rb is a strongly incompatible element, and it can be calculated that the continental crust hosts ~ 55% of the Earth's Rb budget (Rudnick and Gao, 2003; Pringle and Moynier, 2017). Thus, the contribution of the continental crust actually plays a major role in the Rb isotopic composition of the BSE. As mantle partial melting and magmatic processes do not produce significant Rb isotopic fractionation (this study), the continental crust should have similar Rb isotopic characteristics to that of the mantle. This is consistent with the similarity between the estimated Rb isotopic composition of the upper continental crust (-0.14 ± 0.01‰, 2SE, n=73; X. Hu et al., 2022) and our estimation of the mantle's composition (-0.12 ±

615 0.08‰, 2SD; n=25). Given the relative proportions of the crust and mantle, the Rb
616 isotopic composition of the BSE can be estimated through a mass balance calculation:
617 $\delta^{87}Rb_{BSE}=f \times \delta^{87}Rb_{crust}+(1-f) \times \delta^{87}Rb_{mantle}$, where f (~55%, Rudnick and Gao, 2003;
618 Pringle and Moynier, 2017) is the proportion of BSE's Rb budget hosted by the
619 continental crust. The rubidium isotopic composition of the continental crust
620 ($\delta^{87}Rb_{crust}$) is assumed to be represented by the average value of the UCC (-0.14 ±
621 0.09‰, 2SD, n=73; X. Hu et al., 2022), and $\delta^{87}Rb_{mantle}$ to be equal to -0.12 ± 0.08‰
622 (2SD, n=25) as discussed above. Using this approach, the Rb isotopic composition of
623 the BSE is estimated to be -0.13 ± 0.06‰ (2SD; propagated error).
624

625 ## 6. Conclusions

626 In this study, we developed a high precision Rb isotope analytical method on
627 CC-MC-ICP-MS Nu Sapphire. Seven geostandards as well as a synthetic sample
628 (PCC-1+SRM 984) were measured. $\delta^{87}Rb$ values reported here for these standards are
629 all in good agreement with reference data, confirming the accuracy of the method.
630 The long-term reproducibility of Rb isotopic analyses is 0.03‰ (2SD) at 2 ng/g
631 running concentration. Based on this high precision method, a series of igneous rocks
632 from Hekla volcano and 15 MORB samples with various localities were measured.
633 Hekla volcanic rocks exhibit very uniform Rb isotopic composition (from -0.17 to -
634 0.07‰) over a wide range of bulk-rock compositions, ranging from basalts to
635 rhyolites, indicating that Rb isotopic fractionation during magmatic evolution is not
636 significant. Similarly, MORB samples also have a narrow Rb isotopic variation range

(-0.19 to -0.02‰) regardless of their various localities. Combining basaltic samples (MORBs and Hekla basalts) in this study and previously published OIB data, the Rb isotopic composition of the mantle is estimated at -0.12 ± 0.08‰ (2SD, n=25). The average composition of the BSE is evaluated to be -0.13 ± 0.06‰ (2SD), and this is a more precise estimate that is consistent with previous studies.

Acknowledgement

This work was partly supported by the IPGP analytical platform PARI, Region Ile-de-France SESAME Grants no. 12015908, and DIM ACAV +, the ERC grant agreement No. 101001282 (METAL) (F.M.), the UnivEarthS Labex program (numbers: ANR-10-LABX-0023 and ANR-11-IDEX-0005-02) (F.M.). B.W thanks the support of CSC scholarship (No. 202106340025). We are grateful to the editorial handling of Prof. Jeffrey G. Catalano and Prof. Julie Prytulak and constructive comments from Prof. Julie Prytulak, Prof. Oliver Nebel and two anonymous reviewers.

References

Amsellem, E., Moynier, F., Day, J.M., Moreira, M., Puchtel, I.S., Teng, F.-Z., 2018. The stable strontium isotopic composition of ocean island basalts, mid-ocean ridge basalts, and komatiites. Chem. Geol. 483, 595-602.

Badullovich, N., Moynier, F., Creech, J., Teng, F., Sossi, P., 2017. Tin isotopic fractionation during igneous differentiation and Earth's mantle composition. Geochem. Perspect. Lett 5, 24-28.

Bai, R., Jackson, M.G., Huang, F., Moynier, F., Devos, G., Halldórsson, S.A., Lisiecki, L., Yin, H., Peng, Y., Nan, X., 2022. Barium isotopes in ocean island basalts as tracers of mantle processes. Geochim. Cosmochim. Acta 336, 436-447.

Barnes, J.J., Franchi, I.A., McCubbin, F.M., Anand, M., 2019. Multiple reservoirs of volatiles in the Moon revealed by the isotopic composition of chlorine in lunar basalts. Geochim. Cosmochim. Acta 266, 144-162.

Berglund M., Wieser M.E., 2011. Isotopic compositions of the elements 2009 (IUPAC Technical Report). Pure Appl. Chem. 83, 397–410.

Boyce, J.W., Kanee, S.A., McCubbin, F.M., Barnes, J.J., Bricker, H., Treiman, A.H., 2018. Early loss, fractionation, and redistribution of chlorine in the Moon as revealed by the low-Ti lunar mare basalt suite. Earth Planet. Sci. Lett. 500, 205-214.

Boyce J.W., Treiman A.H., Guan Y., Ma C., Eiler J.M., Gross J., Greenwood J.P., Stolper E.M., 2015. The chlorine isotope fingerprint of the lunar magma ocean. Sci. Adv. 1, e1500380.

Chekol, T.A., Kobayashi, K., Yokoyama, T., Sakaguchi, C., Nakamura, E., 2011. Timescales of magma differentiation from basalt to andesite beneath Hekla Volcano, Iceland: Constraints from U-series disequilibria in lavas from the last quarter-millennium flows. Geochim. Cosmochim. Acta 75, 256-283.

Chen, H., Saunders, N.J., Jerram, M., Halliday, A.N., 2021. High-precision potassium isotopic measurements by collision cell equipped MC-ICPMS. Chem. Geol. 578, 120281.

Chen, H., Savage, P.S., Teng, F.-Z., Helz, R.T., Moynier, F., 2013. Zinc isotope fractionation during magmatic differentiation and the isotopic composition of the bulk Earth. Earth Planet. Sci. Lett. 369, 34-42.

Dai, W., Moynier, F., Paquet, M., Moureau, J., Debret, B., Siebert, J., Gerard, Y., Zhao, Y., 2022. Calcium isotope measurements using a collision cell (CC)-MC-ICP-MS. Chem. Geol. 590, 120688.

Day J.M.D. and Moynier F., 2014. Evaporative fractionation of volatile stable isotopes and their bearing on the origin of the Moon. Philos. Trans. R. Soc. Math. Phys. Eng. Sci. 372, 20130259.

Deng Z., Chaussidon M., Savage P., Robert F., Pik R., Moynier F., 2019. Titanium isotopes as a tracer for the plume or island arc affinity of felsic rocks. Proc. Natl. Acad. Sci. 116, 1132–1135.

Deng, Z., Moynier, F., Sossi, P., Chaussidon, M., 2018. Bridging the depleted MORB mantle and the continental crust using titanium isotopes. Geochem. Perspect. Lett 9, 11-15.

Elliott, T., Thomas, A., Jeffcoate, A., Niu, Y., 2006. Lithium isotope evidence for subduction-enriched mantle in the source of mid-ocean-ridge basalts. Nature 443, 565-568.

Gargano, A., Sharp, Z., Shearer, C., Simon, J.I., Halliday, A., Buckley, W., 2020. The Cl isotope composition and halogen contents of Apollo-return samples. Proc. Natl. Acad. Sci. 117, 23418-23425.

Geist, D., Harpp, K., Oswald, P., Wallace, P., Bindeman, I., Christensen, B., 2021. Hekla revisited: fractionation of a magma body at historical timescales. J. Petrol. 62, egab001.

Han, J., Chen, H., Hollings, P., Wang, J., Zhang, D., Zhang, L., Zeng, T., Ma, J., Ai, Y., 2021. Efficient enrichment of Rb during the magmatic-hydrothermal transition in a highly evolved granitic system: Implications from mica chemistry of the Tiantangshan Rb-Sn-W deposit. Chem. Geol. 560, 120020.

Hofmann, A., 2003. Sampling mantle heterogeneity through oceanic basalts: isotopes and trace elements. Treatise on geochemistry 2, 568.

Hu, X., Nan, X., Liu, X., Huang, F., 2022. Rubidium isotope compositions of the average upper continental crust and the Himalayan leucogranites: Implications for magmatic-fluid interaction. Geochim. Cosmochim. Acta 336, 165-176.

Hu, X., Nan, X.-Y., Yu, H.-M., Huang, F., 2021. High precision Rb isotope measurements by MC-ICP-MS. J. Anal. At. Spectrom. 36, 2744-2755.

Hu, Y., Moynier, F., Bizzarro, M., 2022. Potassium isotope heterogeneity in the early Solar System controlled by extensive evaporation and partial recondensation. Nat. Commun. 13, 1-10.

721 Huang, F., Bai, R., Deng, G., Liu, X., Li, X., 2021. Barium isotope evidence for the
722 role of magmatic fluids in the origin of Himalayan leucogranites. Sci. Bull. 66,
723 2329-2336.
724 Inglis, E.C., Moynier, F., Creech, J., Deng, Z., Day, J.M., Teng, F.-Z., Bizzarro, M.,
725 Jackson, M., Savage, P., 2019. Isotopic fractionation of zirconium during
726 magmatic differentiation and the stable isotope composition of the silicate Earth.
727 Geochim. Cosmochim. Acta 250, 311-323.
728 Kato, C., Moynier, F., Valdes, M.C., Dhaliwal, J.K., Day, J., 2015. Extensive volatile
729 loss during formation and differentiation of the Moon. Nat. Commun. 6, 1-4.
730 Klein, E.M., Langmuir, C.H., 1987. Global correlations of ocean ridge basalt
731 chemistry with axial depth and crustal thickness. J. Geophys. Res. Solid Earth
732 92(B8), 8089-8115.
733 Li, W., Cui, M., Pan, Q., Wang, J., Gao, B., Liu, S., Yuan, M., Su, B., Zhao, Y., Teng,
734 F.-Z., 2022. High-precision potassium isotope analysis using the Nu Sapphire
735 collision cell (CC)-MC-ICP-MS. Sci. China Earth Sci. 65, 1510-1521.
736 Liu, Z., Liu, X., Yu, L., Wang, J., 2020. Highly fractionated origin and magmatic-
737 hydrothermal evolution of the Kampa leucogranites in the Tethyan Himalaya. J
738 Nanjing Univ Nat Sci 56, 800-814.
739 Lodders, K., 2003. Solar system abundances and condensation temperatures of the
740 elements. Astrophys. J. 591, 1220.

741 Luck, J.-M., Othman, D.B., Albarède, F., 2005. Zn and Cu isotopic variations in
742 chondrites and iron meteorites: early solar nebula reservoirs and parent-body
743 processes. Geochim. Cosmochim. Acta 69, 5351-5363.
744 McDonough, W.F., Sun, S.-S., 1995. The composition of the Earth. Chem. Geol. 120,
745 223-253.
746 Moune, S., Sigmarsson, O., Thordarson, T., Gauthier, P.-J., 2007. Recent volatile
747 evolution in the magmatic system of Hekla volcano, Iceland. Earth Planet. Sci.
748 Lett. 255, 373-389.
749 Moynier, F., Hu, Y., Wang, K., Zhao, Y., Gérard, Y., Deng, Z., Moureau, J., Li, W.,
750 Simon, J.I., Teng, F.-Z., 2021. Potassium isotopic composition of various
751 samples using a dual-path collision cell-capable multiple-collector inductively
752 coupled plasma mass spectrometer, Nu instruments Sapphire. Chem. Geol. 571,
753 120144.
754 Nan, X., Yu, H., Kang, J., Huang, F., 2022. Re-visiting barium isotope compositions
755 of mid-ocean ridge basalts and the implications. Justc 52, 1-1-1-8.
756 Nebel, O., Mezger, K., van Westrenen, W., 2011a. Rubidium isotopes in primitive
757 chondrites: Constraints on Earth's volatile element depletion and lead isotope
758 evolution. Earth Planet. Sci. Lett. 305, 309-316.
759 Nebel, O., Mezger, K., Scherer, E., Münker, C., 2005. High precision determinations
760 of 87Rb/85Rb in geologic materials by MC-ICP-MS. Int. J. Mass Spectrom. 246,
761 10-18.

762 Nebel, O., Scherer, E.E., Mezger, K., 2011b. Evaluation of the 87Rb decay constant
763 by age comparison against the U–Pb system. Earth Planet. Sci. Lett. 301, 1-8.
764 Nie, N.X., Dauphas, N., 2019. Vapor Drainage in the Protolunar Disk as the Cause for
765 the Depletion in Volatile Elements of the Moon. Astrophys. J. 884, L48.
766 Nie, N.X., Dauphas, N., Hopp, T., Hu, J.Y., Zhang, Z.J., Yokochi, R., Ireland, T.J.,
767 Tissot, F.L., 2021. Chromatography purification of Rb for accurate isotopic
768 analysis by MC-ICPMS: a comparison between AMP-PAN, cation-exchange,
769 and Sr resins. J. Anal. At. Spectrom. 36, 2588-2602.
770 Óskarsson, N., 1981. The chemistry of Icelandic lava incrustations and the latest
771 stages of degassing. J. Volcanol. Geotherm. Res. 10, 93-111.
772 Paniello, R.C., Day, J., Moynier, F., 2012. Zinc isotopic evidence for the origin of the
773 Moon. Nature 490, 376-379.
774 Paquet, M., Moynier, F., Yokoyama, T., Dai, W., Hu, Y., Abe, Y., Aléon, J., O'D
775 Alexander, C.M., Amari, S., Amelin, Y., 2022. Contribution of Ryugu-like
776 material to Earth's volatile inventory by Cu and Zn isotopic analysis. Nat. Astron.
777 7, 182–189.
778 Pringle, E.A., Moynier, F., 2017. Rubidium isotopic composition of the Earth,
779 meteorites, and the Moon: Evidence for the origin of volatile loss during
780 planetary accretion. Earth Planet. Sci. Lett. 473, 62-70.
781 Pringle, E.A., Moynier, F., Beck, P., Paniello, R., Hezel, D.C., 2017. The origin of
782 volatile element depletion in early solar system material: Clues from Zn isotopes
783 in chondrules. Earth Planet. Sci. Lett. 468, 62-71.

784 Prytulak, J., Brett, A., Webb, M., Plank, T., Rehkämper, M., Savage, P., Woodhead, J.,
785 2017. Thallium elemental behavior and stable isotope fractionation during
786 magmatic processes. Chem. Geol. 448, 71-83.
787 Prytulak, J., Sossi, P., Halliday, A., Plank, T., Savage, P., Woodhead, J., 2016. Stable
788 vanadium isotopes as a redox proxy in magmatic systems. Geochem. Perspect.
789 Lett 3, 75-84.
790 Ranta, E.J., Halldórsson, S.A., Barnes, J., Jónasson, K., Stefánsson, A., 2021.
791 Chlorine isotope ratios record magmatic brine assimilation during rhyolite
792 genesis. Geochem. Perspect. Lett. 16, 35-39.
793 Rose-Koga, E.F., Sigmarsson, O., 2008. B–O–Th isotope systematics in Icelandic
794 tephra. Chem. Geol. 255, 454-462.
795 Rudnick, R., Gao, S., Holland, H., Turekian, K., 2003. Treatise on geochemistry.
796 Elsevier Amsterdam, pp. 1-64.
797 Savage, P.S., Georg, R.B., Williams, H.M., Burton, K.W., Halliday, A.N., 2011.
798 Silicon isotope fractionation during magmatic differentiation. Geochim.
799 Cosmochim. Acta 75, 6124-6139.
800 Schilling, J., Zajac, M., Evans, R., Johnston, T., White, W., Devine, J., Kingsley, R.,
801 1983. Petrologic and geochemical variations along the Mid-Atlantic Ridge from
802 29 degrees N to 73 degrees N. Am. J. Sci. 283, 510-586.
803 Schilling, J.G., 1975. Rare-earth variations across ‘normal segments’ of the Reykjanes
804 Ridge, 60–53 N, Mid-Atlantic Ridge, 29 S, and East Pacific Rise, 2–19 S, and

evidence on the composition of the underlying low-velocity layer. J. Geophys. Res. 80, 1459-1473.

Schuessler, J.A., Schoenberg, R., Sigmarsson, O., 2009. Iron and lithium isotope systematics of the Hekla volcano, Iceland—evidence for Fe isotope fractionation during magma differentiation. Chem. Geol. 258, 78-91.

She, J.-X., Kubik, E., Li, W., Moynier, F., 2023. Stable Sn isotope signatures of Mid-ocean ridge basalts. Chem. Geol. 622, 121347.

Sigmarsson, O., Bergþórsdóttir, I.A., Devidal, J.-L., Larsen, G., Gannoun, A., 2022. Long or short silicic magma residence time beneath Hekla volcano, Iceland? Contrib. Mineral. Petrol. 177, 13.

Sigmarsson, O., Condomines, M., Fourcade, S., 1992. A detailed Th, Sr and O isotope study of Hekla: differentiation processes in an Icelandic volcano. Contrib. Mineral. Petrol. 112, 20-34.

Sossi, P.A., Eggins, S.M., Nesbitt, R.W., Nebel, O., Hergt, J.M., Campbell, I.H., O'Neill, H.S.C., Van Kranendonk, M., Davies, D.R., 2016. Petrogenesis and geochemistry of Archean komatiites. J. Petrol. 57, 147-184.

Takazawa, E., Frey, F., Shimizu, N., Obata, M., 2000. Whole rock compositional variations in an upper mantle peridotite (Horoman, Hokkaido, Japan): are they consistent with a partial melting process? Geochim. Cosmochim. Acta 64, 695-716.

Tan, S.H., Horlick, G., 1987. Matrix-effect observations in inductively coupled plasma mass spectrometry. J. Anal. At. Spectrom. 2, 745-763.

827 Tanner, S.D., 1992. Space charge in ICP-MS: calculation and implications.
828 Spectrochim. Acta Part B At. Spectrosc. 47, 809-823.
829 Tartèse, R., Sossi, P.A., Moynier, F., 2021. Conditions and extent of volatile loss from
830 the Moon during formation of the Procellarum basin. Proc. Natl. Acad. Sci. 118,
831 e2023023118.
832 Teng, F.-Z., Dauphas, N., Helz, R.T., 2008. Iron isotope fractionation during
833 magmatic differentiation in Kilauea Iki lava lake. Science 320, 1620-1622.
834 Thorarinsson, S., 1967. The eruption of Hekla 1947–48: the eruption of Hekla in
835 historical times. Soc. Sci. Isl. 1, 1-170.
836 Tian, Z., Chen, H., Fegley Jr, B., Lodders, K., Barrat, J.-A., Day, J.M., Wang, K.,
837 2019. Potassium isotopic compositions of howardite-eucrite-diogenite meteorites.
838 Geochim. Cosmochim. Acta 266, 611-632.
839 Tian, Z., Magna, T., Day, J.M., Mezger, K., Scherer, E.E., Lodders, K., Hin, R.C.,
840 Koefoed, P., Bloom, H., Wang, K., 2021. Potassium isotope composition of
841 Mars reveals a mechanism of planetary volatile retention. Proc. Natl. Acad. Sci.
842 118, e2101155118.
843 Tuller-Ross, B., Savage, P.S., Chen, H., Wang, K., 2019. Potassium isotope
844 fractionation during magmatic differentiation of basalt to rhyolite. Chem. Geol.
845 525, 37-45.
846 Van Kooten, E.M., Moynier, F., Day, J.M., 2020. Evidence for transient atmospheres
847 during eruptive outgassing on the Moon. Planet. Sci. J. 1, 67.

Vollstaedt, H., Mezger, K., Leya, I., 2020. The selenium isotope composition of lunar rocks: Implications for the formation of the Moon and its volatile loss. Earth Planet. Sci. Lett. 542, 116289.

Wang, J., Su, B.-X., Tang, D.-M., Yuan, Q.-H., Li, W.-J., Gao, B.-Y., Bao, Z.-A., Zhao, Y., 2022. High-precision copper isotopic analysis using a Nu Sapphire MC-ICP-MS. J. Anal. At. Spectrom. 37, 2589-2598.

White, W., Klein, E., 2014. 4.13-Composition of the oceanic crust. Treatise on Geochemistry (second edition), 457-496.

Willbold, M., Elliott, T., 2017. Molybdenum isotope variations in magmatic rocks. Chem. Geol. 449, 253-268.

Wing, B.A., Farquhar, J., 2015. Sulfur isotope homogeneity of lunar mare basalts. Geochim. Cosmochim. Acta 170, 266-280.

Wombacher, F., Rehkämper, M., Mezger, K., Bischoff, A., Münker, C., 2008. Cadmium stable isotope cosmochemistry. Geochim. Cosmochim. Acta 72, 646-667.

Workman, R.K., Hart, S.R., 2005. Major and trace element composition of the depleted MORB mantle (DMM). Earth Planet. Sci. Lett. 231, 53-72.

Wu, F., Turner, S., Hoernle, K., Hauff, F., Schaefer, B.F., Kokfelt, T., Bindeman, I., 2023. Barium isotope composition of depleted MORB mantle constrained by basalts from the South Mid-Atlantic Ridge (5–11° S) with implication for recycled components in the convecting upper mantle. Geochim. Cosmochim. Acta 340, 85-98.

Yang, J., Siebert, C., Barling, J., Savage, P., Liang, Y.-H., Halliday, A.N., 2015. Absence of molybdenum isotope fractionation during magmatic differentiation at Hekla volcano, Iceland. Geochim. Cosmochim. Acta 162, 126-136.

Zeng, H., Rozsa, V.F., Nie, N.X., Zhang, Z., Pham, T.A., Galli, G., Dauphas, N., 2019. Ab initio calculation of equilibrium isotopic fractionations of potassium and rubidium in minerals and water. ACS Earth Space Chem. 3, 2601-2612.

Zhang, Z., Ma, J., Wang, Z., Zhang, L., He, X., Zhu, G., Zeng, T., Wei, G., 2021. Rubidium isotope fractionation during chemical weathering of granite. Geochim. Cosmochim. Acta 313, 99-115.

Zhang, Z., Ma, J., Zhang, L., Liu, Y., Wei, G., 2018. Rubidium purification via a single chemical column and its isotope measurement on geological standard materials by MC-ICP-MS. J. Anal. At. Spectrom. 33, 322-328.

Zheng, X.-Y., Chen, X.-Y., Ding, W., Zhang, Y., Charin, S., Gérard, Y., 2022. High precision analysis of stable potassium (K) isotopes by the collision cell MC-ICP-MS “Sapphire” and a correction method for concentration mismatch. J. Anal. At. Spectrom. 37, 1273-1287.

Figure 1. Elution curves for Rb and K of our Sr-spec column chemistry. The homemade heat-shrink Teflon columns (0.46 cm inner diameter, 6.5 cm length)

888 contain 1 mL of Eichrom Sr-spec resin (25–50 μm) and the elution are realized using
889 3 mol/L HNO_3. Relevant data see Supplementary Table 3.

890 **Figure 2.** Rubidium isotopic data of standards. (a): The $\delta^{87}Rb$ of pure NIST SRM 984
891 solution and AGV-2. The long-term reproducibility of Rb isotopic analyses is 0.03‰
892 (2SD) based on the repeated measurements of AGV-2; (b): Rubidium isotopic
893 compositions of one in-house standard IPGP-Rb solution and seven geostandards. The
894 data are reported as $\delta^{87}Rb$ relative to the SRM 984 solution. Data from the literature
895 are reported for comparison.

896 **Figure 3.** Effect of Rb testing concentrations on accuracy and precision. Rubidium
897 concentrations decrease from 10 to 0.5 ng/g for a pure Rb standard as well as for three
898 rock standards (BHVO-2, AGV-2, GSP-2). Relevant data are reported in
899 Supplementary Table 5.

900 **Figure 4.** Effects of concentration and acid molarity mismatch on Rb isotopic
901 measurements. Samples and standards are both pure SRM984 solutions. (a): the
902 bracketing standard was kept at 10 ng/g, samples with different Rb concentrations
903 were prepared to obtain the sample/standard concentration ratio varying from 0.5 to
904 1.5; (b): samples and bracketing standard were prepared with different molarities of
905 acid. Samples were dissolved in HNO_3 from 0.1 moL/L to 1.0 moL/L, while the
906 standard was diluted in 0.5 moL/L HNO_3.

907 **Figure 5.** Matrix effects on Rb isotopic measurements evaluated by doping the
908 solutions with various elements. Rubidium concentrations were set to 2 ng/g, and

[element]/[Rb] represents the concentration ratio of different elements to Rb, e.g., [K]/[Rb]=20 corresponds to K of 40 ng/g.

Figure 6. Rubidium elemental and isotopic characteristics of Hekla volcanic rocks. (a): Rb concentration plotted against SiO_2 content; (b): Rb concentration plotted against MgO content; (c): Rb concentration plotted against K_2O content; (d): Rb concentration plotted against La content; (e): $\delta^{87}Rb$ vs. SiO_2 content; (f): $\delta^{87}Rb$ vs. Rb concentration.

Figure 7. Correlations between $\delta^{87}Rb$ and (a) $(La/Sm)_N$, (b) Rb concentration, (c) MgO content, (d) Na_8 (indicator of partial melting degree which is defined as $Na_8=Na_2O + 0.373 \times MgO - 2.98$; Klein and Langmuir, 1987), and (e) Ba/Th for MORB samples.

Figure 8. Average Rb isotopic composition of the Earth's mantle ($\delta^{87}Rb$=-0.12 ± 0.08‰, 2SD) estimated based on MORBs and Hekla basalts in this study as well as previously reported OIB (Pringle and Moynier, 2017).

Figure 1

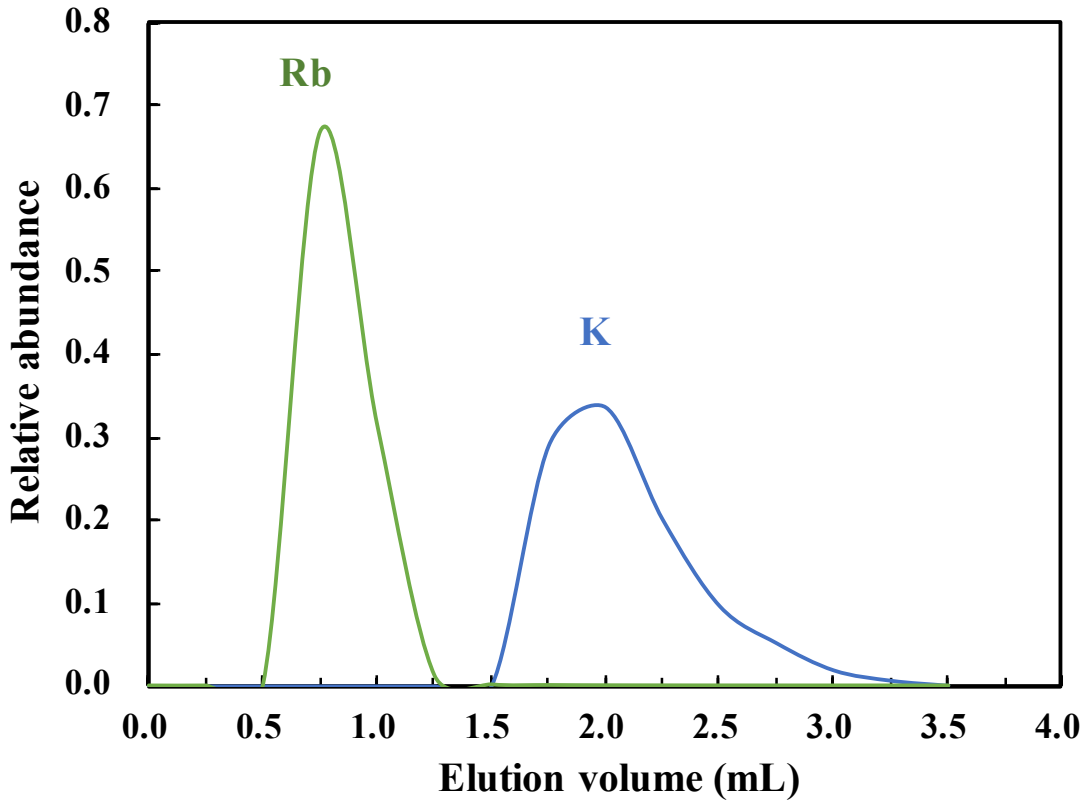
Rb
K
Relative abundance
Elution volume (mL)
0.0
0.1
0.2
0.3
0.4
0.5
0.6
0.7
0.8
0.0
0.5
1.0
1.5
2.0
2.5
3.0
3.5
4.0

Figure 2

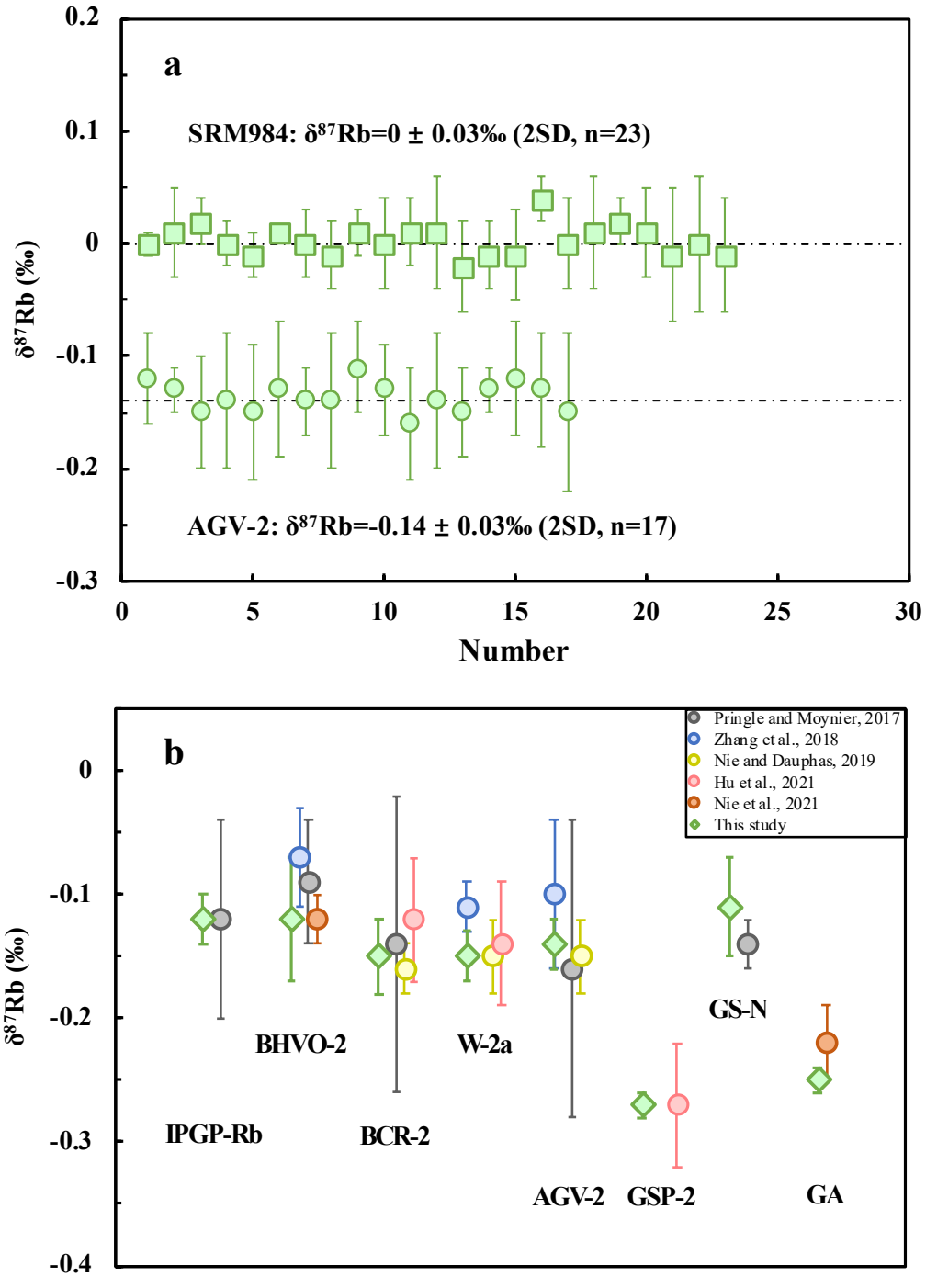
a
SRM984: δ87Rb=0 ± 0.03‰ (2SD, n=23)
AGV-2: δ87Rb=-0.14 ± 0.03‰ (2SD, n=17)
δ87Rb (‰)
Number
b
Pringle and Moynier, 2017
Zhang et al., 2018
Nie and Dauphas, 2019
Hu et al., 2021
Nie et al., 2021
This study
IPGP-Rb
BHVO-2
BCR-2
W-2a
AGV-2
GSP-2
GS-N
GA

Figure 3

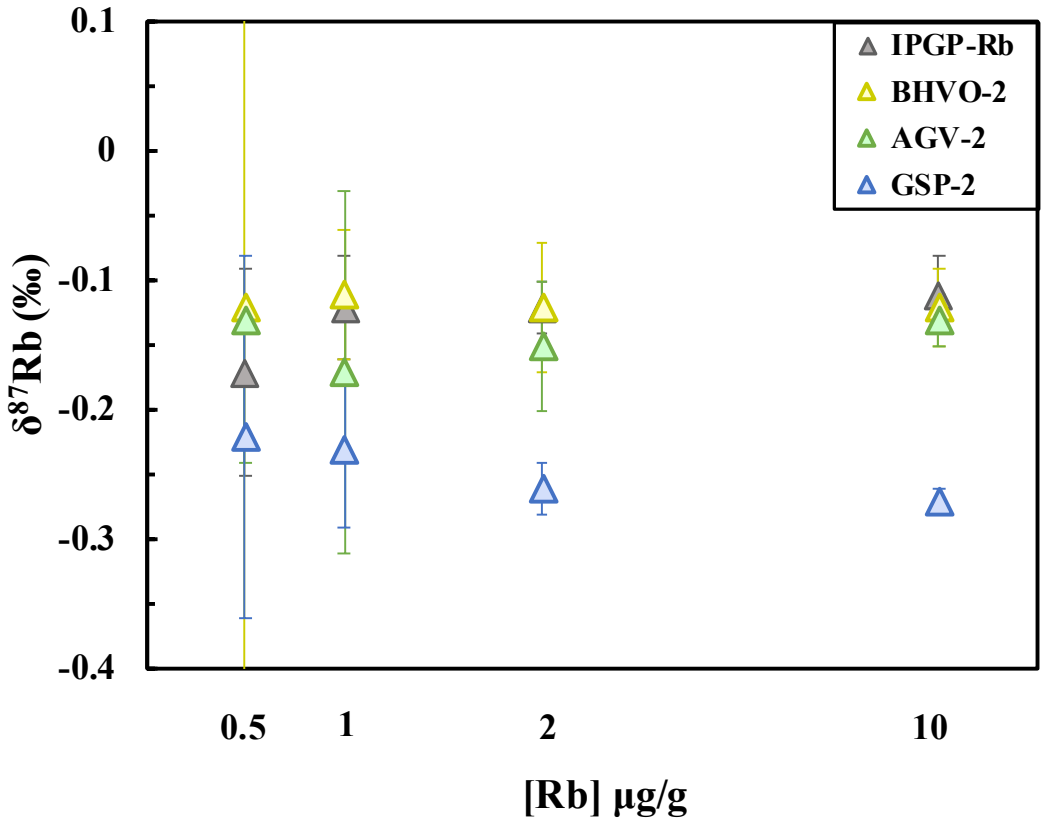

Figure 4

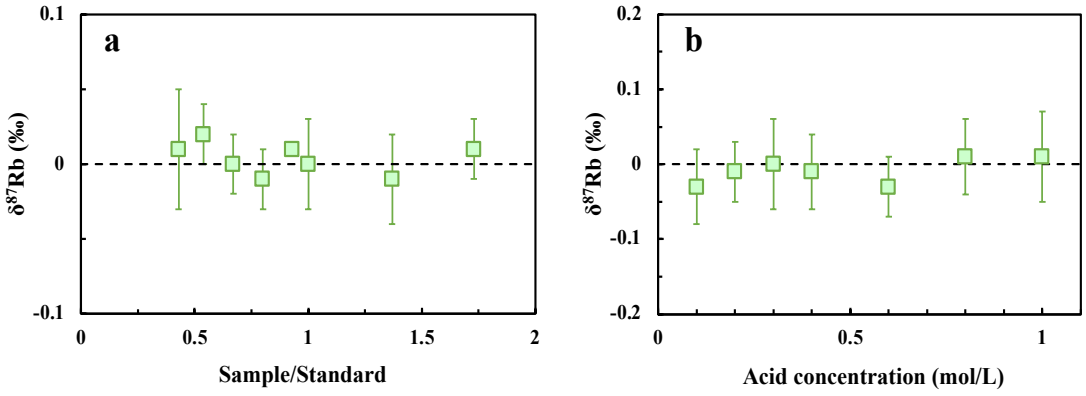

Figure 5

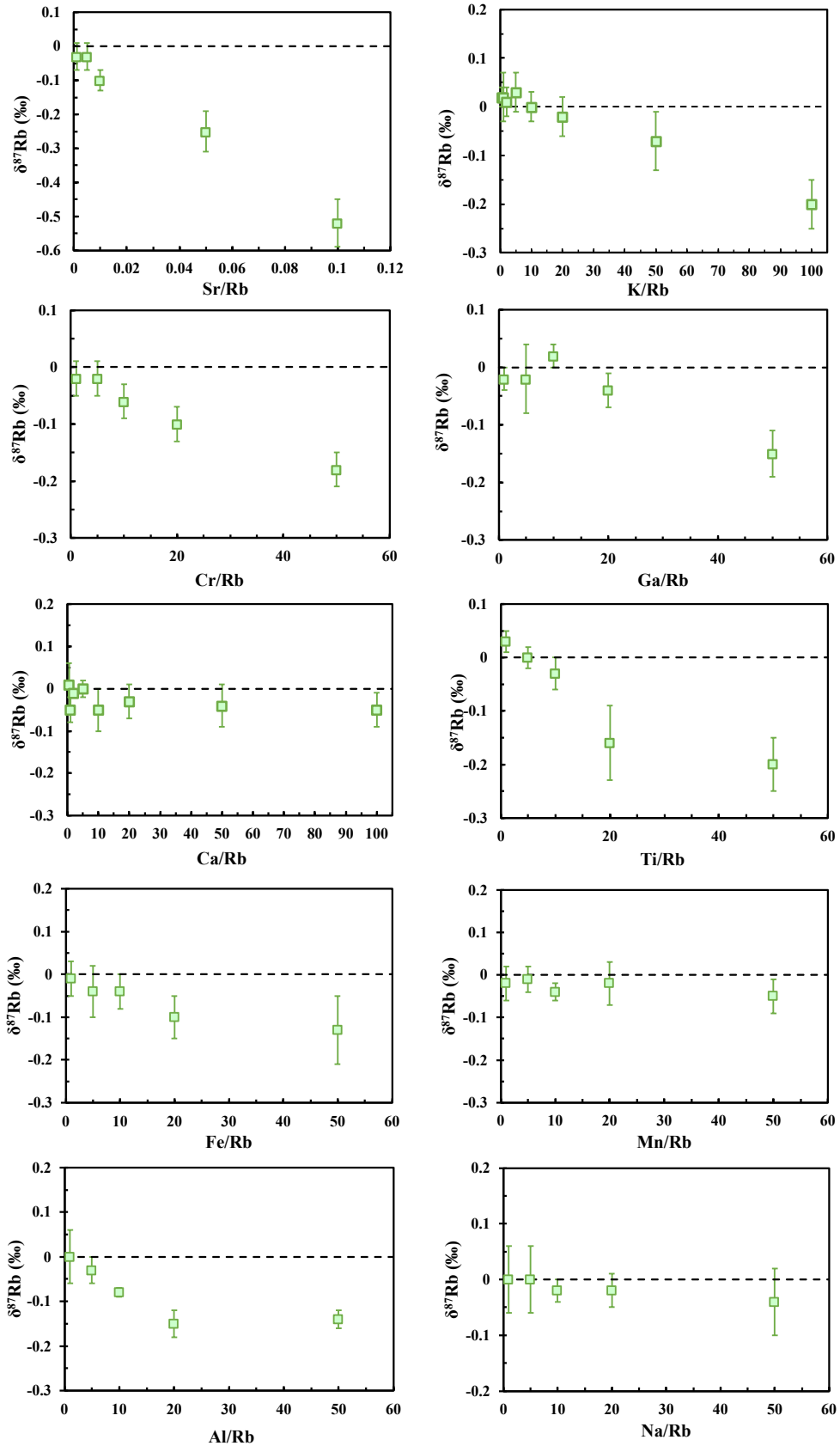

Figure 6

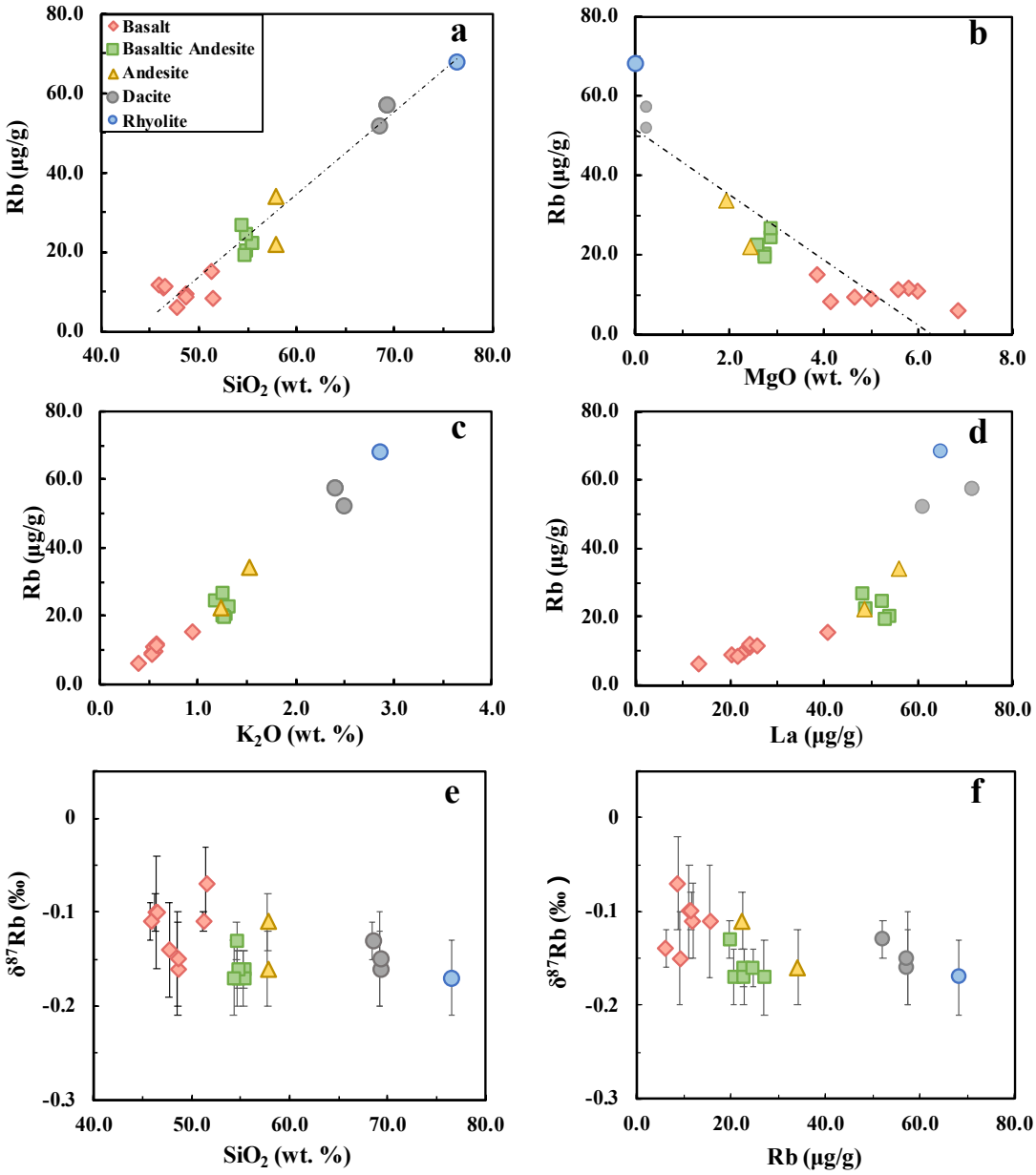
a
Basalt
Basaltic Andesite
Andesite
Dacite
Rhyolite
Rb (μg/g)
SiO2 (wt. %)
b
Rb (μg/g)
MgO (wt. %)
c
Rb (μg/g)
K2O (wt. %)
d
Rb (μg/g)
La (μg/g)
e
δ87Rb (‰)
SiO2 (wt. %)
f
δ87Rb (‰)
Rb (μg/g)

Figure 7

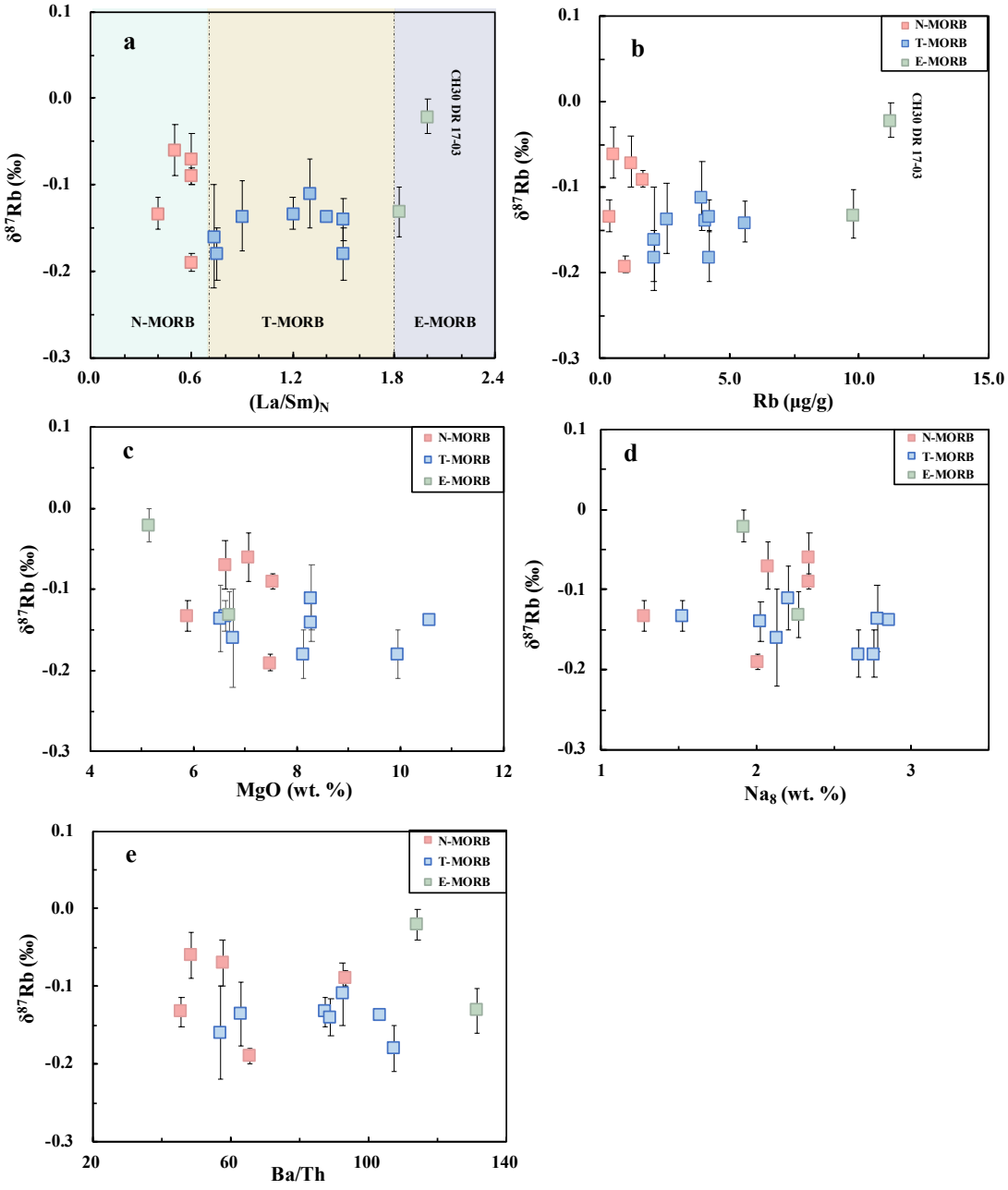
a
N-MORB
T-MORB
E-MORB
CH30 DR 1743
δ87Rb (‰)
(La/Sm)N
b
N-MORB
T-MORB
E-MORB
CH30 DR 1743
δ87Rb (‰)
Rb (μg/g)
c
N-MORB
T-MORB
E-MORB
δ87Rb (‰)
MgO (wt. %)
d
N-MORB
T-MORB
E-MORB
δ87Rb (‰)
Na8 (wt. %)
e
N-MORB
T-MORB
E-MORB
δ87Rb (‰)
Ba/Th

Figure 8

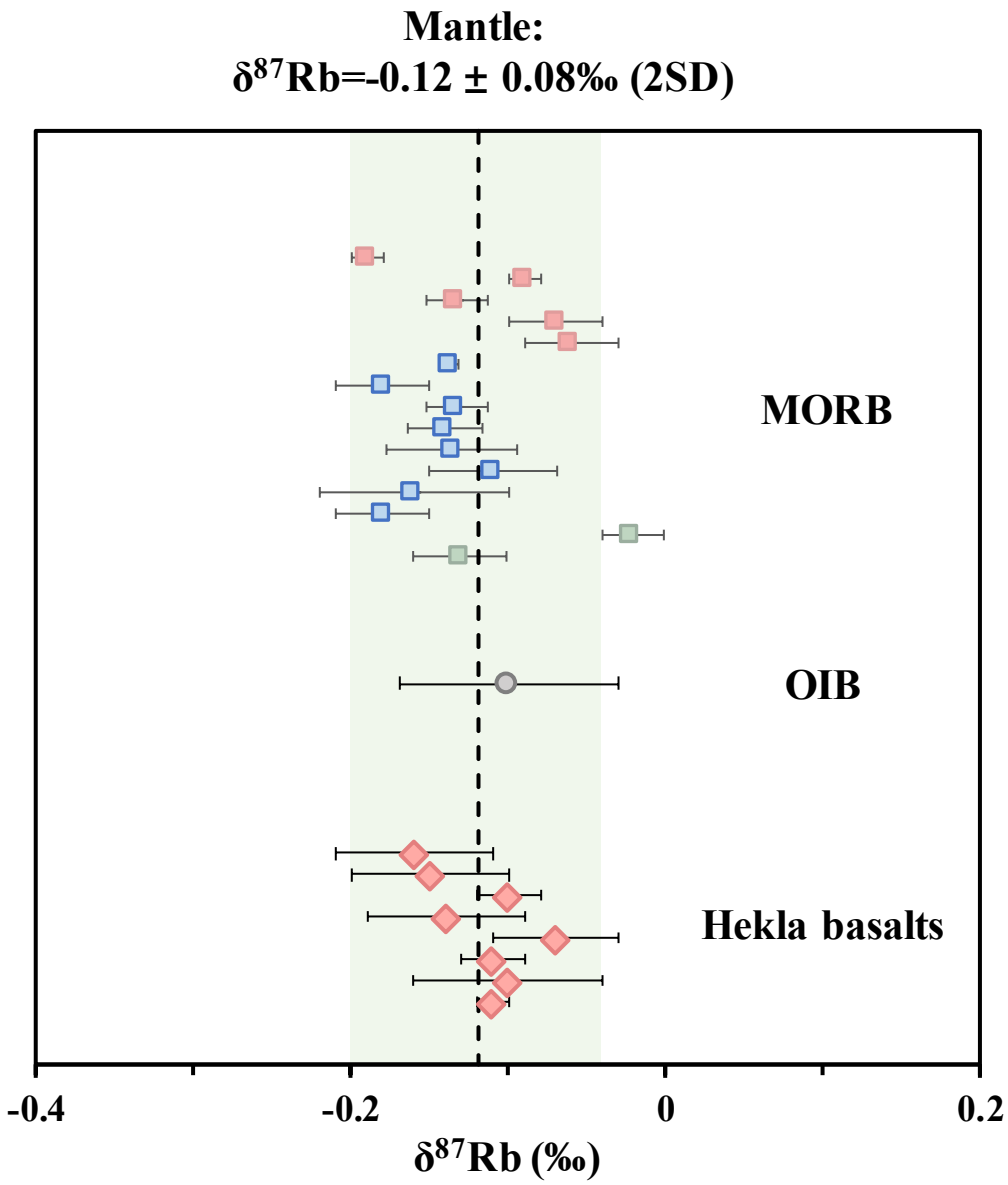
Mantle:
δ87Rb=-0.12 ± 0.08‰ (2SD)
MORB
OIB
Hekla basalts
-0.4
-0.2
0
0.2
δ87Rb (‰)

Table 1. Rubidium isotopic compositions of standards.

	This study		*Reference value*		
Standard	δ^{87}Rb (‰)	2SD	δ^{87}Rb (‰)	2SD	Literature
IPGP-Rb	-0.12	0.02	-0.12	0.08	Pringle and Moynier (2017)
BHVO-2	-0.12	0.05	-0.12	0.02	Nie et al. (2021)
			-0.09	0.05	Pringle and Moynier (2017)
			-0.07	0.04	Zhang et al. (2018)
BCR-2	-0.15	0.03	-0.12	0.03	Hu et al. (2021)
			-0.14	0.12	Pringle and Moynier (2017)
			-0.16	0.02	Nie and Dauphas (2019)
W-2a	-0.15	0.02	-0.14	0.05	Hu et al. (2021)
			-0.11	0.02	Zhang et al. (2018)
			-0.15	0.03	Nie and Dauphas (2019)
AGV-2	-0.14	0.02	-0.16	0.12	Pringle and Moynier (2017)
			-0.10	0.06	Zhang et al. (2018)
			-0.15	0.03	Nie and Dauphas (2019)
GSP-2	-0.27	0.01	-0.27	0.02	Hu et al. (2021)
GS-N	-0.11	0.04	-0.14	0.02	Pringle and Moynier, 2017
GA	-0.25	0.01	-0.22	0.03	Nie et al. (2021)

Table 2. Rubidium isotopic compositions of Hekla volcanic rocks.

Sample	Type	SiO_2 (wt. %)	MgO (wt. %)	K_2O (wt. %)	La (μg/g)	Rb (μg/g)	$\delta^{87}Rb$ (‰)	2SD[a]	n
ICE 20-22	Basalt	48.59	4.66	0.56	22.7	9.8	-0.16	0.05	4
ICE 20-25	Basalt	48.60	5.00	0.54	20.1	9.2	-0.15	0.05	4
ICE 20-28	Basalt	46.27	6.00	0.55	24.1	11.2	-0.10	0.02	3
ICE 20-31	Basalt	47.71	6.83	0.39	13.1	6.2	-0.14	0.05	4
ICE 20-36	Basalt	51.44	4.16	0.54	21.4	8.7	-0.07	0.04	3
ICE 20-37	Basalt	45.80	5.80	0.58	24.0	11.9	-0.11	0.02	3
ICE 20-41	Basalt	46.44	5.58	0.58	25.8	11.6	-0.10	0.06	4
ICE 20-45	Basalt	51.20	3.84	0.95	40.5	15.5	-0.11	0.01	3
ICE 20-19	Basaltic Andesite	54.70	2.75	1.28	53.9	20.6	-0.17	0.03	3
ICE 20-23	Basaltic Andesite	55.34	2.58	1.31	48.6	22.7	-0.16	0.02	3
ICE 20-23 (Replicate[b])	Basaltic Andesite	55.34	2.58	1.31	48.6	22.7	-0.17	0.03	3
ICE 20-34	Basaltic Andesite	54.59	2.76	1.27	52.7	19.7	-0.13	0.02	3
ICE 20-40	Basaltic Andesite	54.72	2.88	1.18	52.0	24.7	-0.16	0.02	3
ICE 20-44	Basaltic Andesite	54.27	2.87	1.25	48.0	27.0	-0.17	0.04	3
ICE 20-24	Andesite	57.76	2.42	1.24	48.3	22.4	-0.11	0.03	3
ICE 20-35	Andesite	57.77	1.91	1.53	55.9	34.1	-0.16	0.04	3
ICE 20-32	Dacite	69.21	0.24	2.41	71.6	57.4	-0.16	0.04	3
ICE 20-32 (Replicate[b])	Dacite	69.21	0.24	2.41	71.6	57.4	-0.15	0.05	3
ICE 20-39	Dacite	68.43	0.24	2.49	61.0	52.1	-0.13	0.02	3
ICE 20-33	Rhyolite	76.52	0.02	2.87	64.8	68.3	-0.17	0.04	3

[a]2SD = 2 times the standard deviation of the population of three repeat measurements of a sample solution;

[b] Replicate = repeat chemical purification and measurement of different aliquots of a stock solution.

Table 3. Rubidium isotopic compositions of MORB samples.

Sample	Location	MgO[a] (wt. %)	$(La/Sm)_N$[a]	Na_8[a] (wt. %)	Ba/Th[a]	Rb[a] (μg/g)	$\delta^{87}Rb$ (‰)	2SD	n
CYP78 12-34	East Pacific Ridge	7.53	0.6	2.34	93.2	1.7	-0.09	0.01	4
SEARISE1 DR04	East Pacific Ridge	6.61	0.6	2.08	57.6	1.2	-0.07	0.03	4
SEARISE2 DR03	East Pacific Ridge	7.06	0.5	2.34	48.4	0.5	-0.06	0.03	4
CYP74 31-35	Mid Atlantic Ridge	10.56	1.4	2.86	103.3	4.0	-0.14	0.01	3
ARP 73 13 4	Mid Atlantic Ridge	9.95	1.5	2.66	107.2	4.2	-0.18	0.03	3
ARP 74 9 13C COLUMN	Mid Atlantic Ridge	6.61	1.2	1.53	87.3	4.2	-0.13	0.02	3
ARP 74 7 8 SURFACE	Mid Atlantic Ridge	8.28	1.5	2.03	88.9	5.6	-0.14	0.02	3
DSDP-52-417D-55-2	Mid Atlantic Ridge	5.89	0.4	1.28	45.6	0.4	-0.13	0.02	3
CH30 DR 17-03	Mid Atlantic Ridge	5.15	2.0	1.92	114.0	11.2	-0.02	0.02	3
CH30 DR 17-03 (Replicate)	Mid Atlantic Ridge	5.14	2.0	1.92	114.0	11.2	0.01	0.04	3
CH31-DR12-137	Mid Atlantic Ridge	8.28	1.3	2.21	92.3	3.9	-0.11	0.04	4
EW9309 3D-1g	Mid Atlantic Ridge	6.69	1.8	2.28	131.3	9.8	-0.13	0.03	3
MD57 D6-7	Central Indian Ridge	8.13	0.8	2.76	83.3	3.0	-0.18	0.03	4
MD57 D3-3	Central Indian Ridge	7.48	0.6	2.01	65.4	1.0	-0.19	0.01	3
MD34 D1	Central Indian Ridge	6.52	0.9	2.78	62.8	2.6	-0.14	0.04	3
MD57 D13	Central Indian Ridge	6.76	0.7	2.13	56.9	2.1	-0.16	0.06	3

[a] Major and trace elements data is from She et al. (2023).